JOURNAL OF GEOPHYSICAL RESEARCH, VOL. 107, NO. A11, 1362, doi:10.1029/2002JA009245, 2002

Solar wind dependence of the occurrence and motion of polar auroral arcs: A statistical study

A. Kullen
Royal Institute of Technology, Alfvén Laboratory, Stockholm, Sweden

M. Brittnacher
Department of Earth and Space Sciences, University of Washington, Seattle, Washington, USA

J. A. Cumnock[1] and L. G. Blomberg
Royal Institute of Technology, Alfvén Laboratory, Stockholm, Sweden

Received 4 January 2002; revised 15 March 2002; accepted 25 March 2002; published 14 November 2002.

[1] Polar UV images from a 3-month period in winter 1998–1999 are used for a statistical study of polar arcs. The study covers all auroral arcs that are located poleward of the northern auroral oval, and which are detectable by the UV imager. The arcs are examined with respect to their spatial and temporal behavior as well as to a possible connection to solar wind parameters using ACE satellite data. It is found that the majority of polar arcs appear during northward IMF, strong IMF magnitude, and high solar wind speed. A modified Akasofu-Perreault epsilon parameter with a cosine function instead of a sine function ($vB^2 \cos^4(\theta/2)(l_0^2/\mu_0)$) combines these results. It correlates well with the occurrence frequency of polar arcs for long timescales. The location of polar arcs is strongly dependent on the sign of the IMF B_y component. Static polar arcs occur in the Northern Hemisphere on the dawn (dusk) side of the oval for negative (positive) IMF B_y, whereas poleward-moving arcs separate from the opposite side of the oval, and then move in the direction of IMF B_y. All polar arcs are sorted into five different categories according to their spatial structure and evolution: oval-aligned, bending, moving, midnight, and multiple arcs. Each polar arc type occurs for a characteristic combination of solar wind parameters. IMF clock angle changes seem to have a strong influence on what type of arc occurs. Oval-aligned arcs appear mainly during steady IMF, bending arcs after an IMF B_z sign change, and moving arcs after an IMF B_y sign change. For the rare midnight and multiple arc events, no characteristic IMF clock angle dependence has been found. The different types of clear polar arcs are discussed in the context of existing observational studies and transpolar arc models. *INDEX TERMS:* 2475 Ionosphere: Polar cap ionosphere; 2736 Magnetospheric Physics: Magnetosphere/ionosphere interactions; 2784 Magnetospheric Physics: Solar wind/magnetosphere interactions; 2776 Magnetospheric Physics: Polar cap phenomena; *KEYWORDS:* Polar arc, transpolar arc, solar wind, IMF, transpolar arc model

Citation: Kullen, A., M. Brittnacher, J. A. Cumnock, and L. G. Blomberg, Solar wind dependence of the occurrence and motion of polar auroral arcs: A statistical study, *J. Geophys. Res.*, *107*(A11), 1362, doi:10.1029/2002JA009245, 2002.

1. Introduction

1.1. Definition of Polar Arcs

[2] Polar arcs are defined as high-latitude auroral arcs located poleward of the main auroral oval. There are several types of polar arcs and differences are, for example, found in their spatial extent and in their magnetospheric source regions. Small-scale Sun-aligned arcs occur at high latitudes and have a length of only a few hundred kilometers. While several authors propose that small-scale Sun-aligned arcs occur on open field lines [e.g., *Gussenhoven and Mullen*, 1989, and references therein] others claim that their source regions remain unclear [*Bonnell et al.*, 1999].

[3] Large-scale polar arcs are several hundred kilometers wide and extend from about 1000 km to the entire diameter of the polar cap in length. A multitude of different large-scale polar arc formations have been found and various names have been used to describe these. Large-scale arcs which stretch over the entire polar cap connecting the nightside with the dayside oval are called transpolar arcs [*Frank et al.*, 1982, 1986]. They have similar particle characteristics to those along the main oval, which suggests an origin in the plasma sheet or plasma sheet boundary layer

[1] Also at Center for Space Sciences, University of Texas, Richardson, Texas, USA.

Copyright 2002 by the American Geophysical Union.
0148-0227/02/2002JA009245$09.00

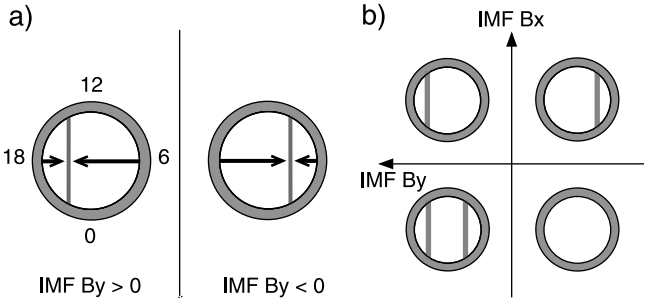

Figure 1. Statistical results of (a) IMF B_y dependent motion of small-scale Sun-aligned arcs by *Valladares et al.* [1994] and (b) IMF B_y and B_x dependent location of oval-aligned arcs by *Elphinstone et al.* [1990].

[e.g., *Meng*, 1981; *Peterson and Shelley*, 1984; *Frank et al.*, 1986; *Frank and Craven*, 1988; *Huang et al.*, 1987, 1989]. Occasionally large-scale arcs can be hook-shaped with the arc connected to the auroral oval only in the midnight sector [*Ismail and Meng*, 1982; *Murphree et al.*, 1982] or near noon [*Gusev and Troshichev*, 1986]. Static transpolar arcs near the dawnside or duskside auroral oval are sometimes referred to as oval-aligned arcs [*Murphree and Cogger*, 1981]. The so-called horse-collar aurora describes oval-aligned arcs at the dawn and dusk poleward edges of an expanded oval [*Hones et al.*, 1989]. A few cases have been reported where a transpolar arc does not separate from the dawnside or duskside oval but grows from the nightside oval. *Craven et al.* [1986] presented an example where a single arc starts at midnight and stretches toward noon. According to *McEwen and Zhang* [2000], such events are rare. *Brittnacher et al.* [1999] found a case during a major magnetic storm where multiple large-scale polar arcs fill the whole polar cap. One of the arcs develops clearly from the nightside oval. As pointed out in the review paper by *Zhu et al.* [1997] it is not yet clear whether different polar arcs represent the same auroral phenomena (but described differently depending on the means of observations) or whether these are fundamentally different types of polar arcs.

1.2. IMF Control of Polar Arcs

[4] The occurrence of polar arcs is strongly controlled by the interplanetary magnetic field (IMF). From numerous studies it is known that polar arcs are a predominantly northward IMF phenomenon, which includes small-scale Sun-aligned arcs [e.g., *Lassen and Danielsen*, 1978; *Gussenhoven*, 1982; *Ismail and Meng*, 1982] and transpolar arcs [e.g., *Frank et al.*, 1986]. The existence of transpolar arcs which appear during southward IMF has been explained by *Frank and Craven* [1988] as arcs which have formed during northward IMF conditions but persist for some time following a change to southward IMF (corresponding to the time span necessary to reconfigure the tail). In a large statistical study about small-scale Sun-aligned arcs based on images from ground-based all-sky cameras (ASIP) in the Northern Hemisphere *Valladares et al.* [1994] came to the same conclusion.

[5] Another result by *Valladares et al.* [1994] refers to the arc location in the polar cap. Small-scale Sun-aligned arcs occur preferably on the dawn side, less often on the dusk side, which confirms earlier results for both the northern [*Ismail et al.*, 1977; *Gussenhoven*, 1982] and the southern polar cap [*Rairden and Mende*, 1989]. Whether this preference is true for large-scale polar arcs remains to be shown.

[6] The IMF B_y component controls the motion of polar arcs. The statistical study of *Valladares et al.* [1994] shows the correlation between polar arc motion and IMF B_y component in the Northern Hemisphere. They found that the dawn-dusk component of the IMF causes a motion of most small-scale Sun-aligned arcs in the direction of IMF B_y. However, the arcs near the side of the auroral oval which lies in the direction of IMF B_y move slightly in the opposite direction (Figure 1a). The motion of transpolar arcs is controlled by IMF B_y in the same way as the small-scale Sun-aligned arcs. *Frank et al.* [1985] reported a dusk to dawn moving transpolar arc for dawnward IMF B_y and, conversely, *Huang et al.* [1989] reported a duskward moving transpolar arc for duskward directed IMF B_y. The observational study by *Craven et al.* [1991] of two simultaneously appearing transpolar arcs in both hemispheres indicates that the motion of transpolar arcs in the southern hemisphere is in the opposite direction. Probably, even small-scale Sun-aligned arcs of the southern polar cap move in the opposite direction, but this remains to be shown. It is expected from the results described above that oval-aligned arcs in the Northern Hemisphere are located on the side of the oval to which IMF B_y is pointing. *Elphinstone et al.* [1990] though, found a different correlation between (mainly oval-aligned) large-scale polar arcs and IMF. In their study of polar cap size and location during northward IMF based on VIKING images of the Northern Hemisphere the location of polar arcs are related to 1-hour averaged IMF B_y and B_x components. They found that duskside arcs occur for duskward IMF B_y only, independent of IMF B_x but that dawnside arcs occur for B_y and B_x having opposite signs. This means, dawnside oval-aligned arcs occur even for duskward IMF B_y (Figure 1b).

[7] The sign of the IMF B_x component may influence the occurrence probability of polar arcs. *Lassen and Danielsen* [1978] reported that small-scale Sun-aligned arcs occur more frequently during periods of negative IMF B_x in the Northern Hemisphere. In the Southern Hemisphere the opposite sign of IMF B_x seems to be favorable for the occurrence of auroral activity in the polar cap. A statistical study of field-aligned currents in the dayside polar cap of the southern hemisphere by *Iijima et al.* [1984] shows a strong correlation between the current densities and positive IMF B_x. These field-aligned currents inside the polar cap are referred to as NBZ (northward B_z) currents as they are shown to be a predominantly northward IMF phenomenon. The existence of strong NBZ currents is likely to be an indication of the appearance of polar arcs as polar arcs are always associated with field-aligned currents [e.g., *Zhu et al.*, 1997, and references therein].

[8] Several papers have reported an influence of IMF sign changes on the appearance of transpolar arcs. Both *Newell et al.* [1997] and *Chang et al.* [1998] presented observations of transpolar arcs which appear when an IMF B_z sign change takes place. In their studies, the motion of the transpolar arc is IMF B_y dependent but it is the rotation of the IMF to southward B_z that causes the transpolar arc to initially appear. In their observations, the IMF B_z southward

period lasts for at least 10 min which questions earlier results about polar arcs being a purely northward IMF phenomenon. A sign change of IMF B_y has been reported as another cause of transpolar arcs. *Cumnock et al.* [1997] and *Chang et al.* [1998] both show several events where a transpolar arc separates from one side of the oval after an IMF B_y sign change and moves poleward. In a recent paper by *Cumnock et al.* [2002] transpolar arcs are examined which appear for IMF B_y sign changes during purely northward IMF B_z. All those studies find that Northern Hemisphere transpolar arcs which are triggered by either an IMF B_y or an IMF B_z sign change separate from the side of the oval which is opposite to the IMF B_y direction.

1.3. Solar Wind–Magnetospheric Coupling and Polar Arcs

[9] As polar arcs are predominantly a northward IMF phenomenon they appear preferably during quiet geomagnetic times with low K_P and AE values [e.g., *Ismail et al.*, 1977]. The negative correlation between AE index and polar arc occurrence is confirmed in the statistical study of *Lassen and Danielsen* [1989]. They even show that for AE decreasing below 30 nT Sun-aligned polar arcs tend to increase in length, stretching across the polar cap. The coupling between AE index and solar wind parameters has been studied extensively and several coupling parameters have been proposed during the last 20 years such as the Akasofu-Perreault epsilon parameter ($vB^2 \sin^4(\theta/2)(l_0^2/\mu_0)$) [*Perreault and Akasofu*, 1978]. The good correlation between epsilon and the AE index on long timescales has been confirmed [e.g., *Akasofu*, 1980]. The current density of the region 1 current system seems to be correlated to this type of solar wind coupling parameter as well. *Iijima and Potemra* [1982] find the best correlation between region 1 current densities and solar wind parameters for a function similar to the epsilon parameter ($(B_y^2 + B_z^2)^{1/2} \sin(\frac{\theta}{2})$). The complementary parameter ($(B_y^2 + B_z^2)^{1/2} \sin(\frac{\theta}{2})$) which they denote as ϵ^* is shown to be strongly correlated to the NBZ current system on the dayside part of the polar cap [*Iijima et al.*, 1984]. ϵ^* is likely to also correlate to field-aligned currents associated with polar arcs.

1.4. Models of Transpolar Arcs

[10] If one were to trace the magnetic field lines from a transpolar arc into the magnetotail in a standard configuration of the magnetosphere with a butterfly shaped plasma sheet centered about the equatorial plane, the transpolar arc field lines would map into the lobes. This is, however, not supported by observations. As mentioned before, transpolar arcs have their origin in the plasma sheet or its boundary layer. Thus, the plasma sheet must have a different shape during the occurrence of transpolar arcs. Several different tail topologies have been proposed to explain the observations.

[11] *Frank et al.* [1982] suggested that the tail plasma sheet is bifurcated such that a north-south aligned plasma sheet bulge extends into the lobes. *Huang et al.* [1987, 1989] found observations that are consistent with filamentary extensions of the plasma sheet into the lobes rather than one large-scale bulge.

[12] Another model, first proposed by *Meng* [1981], interprets transpolar arcs occurring for nonzero IMF B_y as the poleward boundary of an expanded auroral oval. The poleward expansion of the oval corresponds to the thickening of the plasma sheet. This model requires a highly contracted polar cap and a dawn-dusk asymmetry or a twisting of the plasma sheet [*Makita et al.*, 1991]. The now well-known connection between a strong dawn-dusk IMF component and a twist of the entire magnetotail [e.g., *Kaymaz et al.*, 1994, and references therein] supports twisting of the plasma sheet, shown in Figure 2a, as a more probable alternative. The twisted tail plasma sheet causes the open/closed field line boundary in the northern ionosphere to extend poleward on the duskside (dawnside) of the oval for positive (negative) IMF B_y [*Cowley*, 1981; *Kullen and Blomberg*, 1996]. Assuming the poleward boundary of the auroral oval to roughly overlap with the boundary between open and closed field lines the northern auroral oval is expected to broaden at the duskside (dawnside) of the oval for positive (negative) IMF B_y. Polar arcs are expected to lie on the poleward boundary of the expanded side of the oval.

[13] MHD simulations show that an IMF B_y induced twisting of the tail plasma sheet is not equally strong for northward and southward IMF. Only for northward IMF large twists occur [e.g., *Walker et al.*, 1999]. A statistical study of *Owen et al.* [1995] of the structure of the distant magnetotail confirms the MHD results. If the plasma sheet twist plays a major role for the appearance of transpolar arcs, the observation of strong twists for northward IMF may explain why transpolar arcs occur predominantly during northward IMF. The simultaneous occurrence of transpolar arcs on opposite sides of the noon-midnight meridian in the Northern and Southern Hemisphere [*Gusev and Troshichev*, 1986; *Craven et al.*, 1991] is another indication of the influence of a symmetrically twisted tail around the Earth-Sun line on the location of transpolar arcs.

[14] *Kullen* [2000] developed a model which explains the occurrence and motion of transpolar arcs following an IMF B_y sign change with a rotation of the tail twist. The model is based on the assumption that an IMF B_y sign change causes the magnetotail to change the direction of its twist successively such that in an intermediate state the near-Earth tail and the distant tail are twisted in opposite directions. Such a topology leads to a bifurcation of closed field lines in the near-Earth tail which in this model is responsible for the occurrence of a transpolar arc. To demonstrate this, the T89 model [*Tsyganenko*, 1989] has been modified to model the assumed tail topology. Mapping from the model tail current sheet into the ionosphere shows a region of closed field lines stretching into the polar cap which may be interpreted as the location of a transpolar arc. Figure 2b is a schematic showing how a rotated plasma sheet twist forces the region of closed field lines to bifurcate in the near-Earth region. The bifurcated part of the closed field lines originates in the far tail from the flank of the plasma sheet which stretches to very high latitudes. Following these field lines earthward they map into the high lobes of the oppositely twisted near-Earth tail. The poleward motion of the arc is caused by the tail twist reversal propagating tailward such that the high-latitude flank from the far tail maps increasingly poleward. The model by *Kullen* [2000] differs from the ''plasma sheet bifurcation'' model in that the region of closed field lines is bifurcated but not the plasma sheet itself. Recent MHD

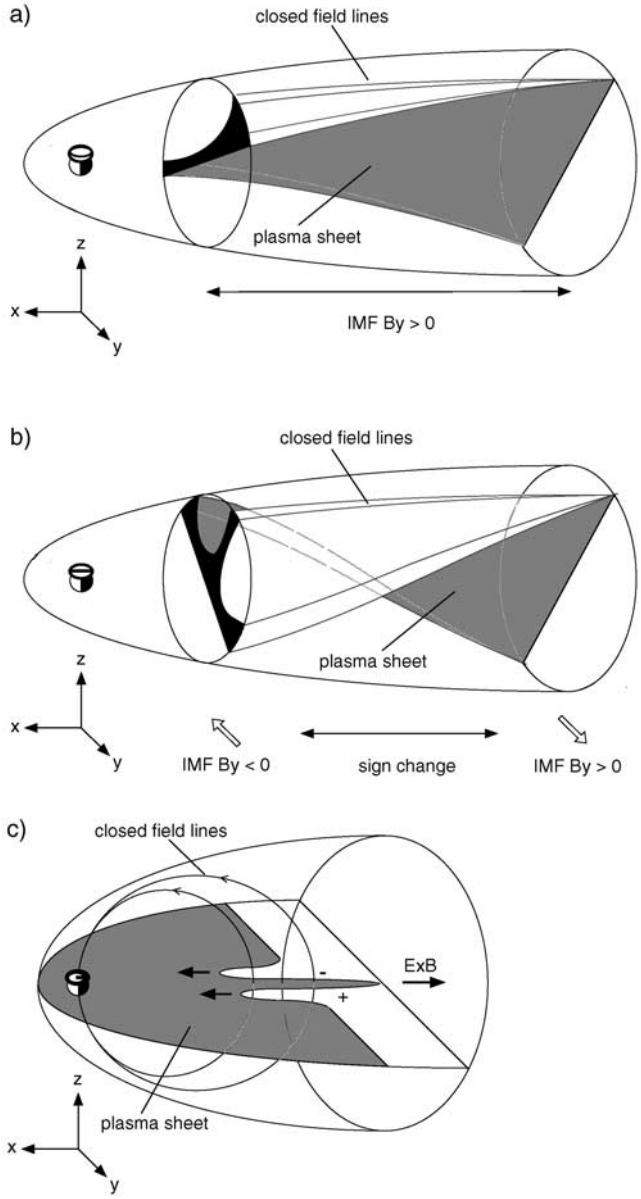

Figure 2. Schematic of different polar arc models illustrating the tail topology and closed field line region for the Northern Hemisphere. (a) Tail model for oval-aligned arcs [*Makita et al.*, 1991]: An IMF B_y induced tail twist causes the high-latitude flank to map to a stationary polar arc. (b) Tail model for moving arcs [*Kullen*, 2000]: A rotation of the tail twist caused by an IMF B_y sign change leads to a bifurcation of the closed field line region in the near-Earth tail. The bifurcated region maps to a transpolar arc which moves from one side of the oval to the other while the rotation of the tail twist propagates tailward. (c) Tail model for midnight arcs [*Rezhenov*, 1995]: An interchange instability causes a tailward moving plasma sheet tongue. This tongue maps to a polar arc which grows from midnight to noon.

simulations by *Slinker et al.* [2001] confirm the assumption that the IMF B_y sign change leads to a rotation of the tail twist. Ionospheric mapping plots show a bar of closed field lines moving over the entire polar cap.

[15] A different transpolar arc model has become established in recent years. *Newell et al.* [1997] proposed a model based on the idea of an abruptly moving dayside reconnection line after an IMF B_z flip. The sudden displacement of the merging line is assumed to lead to a new region of open field lines equatorward of the polar cap which, depending on the IMF B_y component, is located on the prenoon or postnoon side of the oval. *Chang et al.* [1998] refined this model and extended it to IMF B_y sign changes. These ideas are an extension of the theory explaining poleward moving auroral forms which split from the dayside auroral oval and move within some minutes poleward until they disappear. Poleward moving auroral forms begin to appear after the IMF turns southward and continue to occur transiently as long as a weakly southward IMF orientation is maintained. They are interpreted as the optical signature of transient reconnection pulses on the dayside magnetopause which are assumed to cause additional regions of new open flux on the front of the polar cap [*Sandholt et al.*, 1998; *Milan et al.*, 2000].

[16] *Rezhenov* [1995] proposed a model to explain large-scale polar arcs growing from the nightside toward the dayside with an interchange instability inside the magnetotail (Figure 2c). He suggests that such arcs occur during substorm recovery and strong northward IMF and/or high solar wind velocity leading to a short plasma sheet and a highly dipolarized tail magnetic field. According to his model strongly curved magnetic field lines cause a dusk to dawn current in the plasma sheet. A small distortion at the tailward plasma sheet boundary leads to a charge separation. An E $\times$ B drift causes the displacement to grow tailward, i.e., an interchange instability occurs. A tongue of plasma moves tailward which maps to a growing midnight arc.

1.5. The Goal of This Study

[17] This Polar UVI study focuses on the IMF control and possible IMF triggers of polar arcs with the goal of understanding the sometimes contradicting results that have been presented in the literature. One of the reasons for the confusion is that statistical results exist only for small-scale Sun-aligned arcs and not for large-scale polar arcs, a fact not always realized by authors when discussing polar arcs. Another reason may be that in most papers the history of the IMF before the arc occurrence is not considered. Here, a period of 3 months is examined in order to detect every polar arc which is visible on the UV images. With a limited spatial resolution and energy range, only bright large-scale arcs can be detected, and thus small-scale Sun-aligned arcs do not appear in this study. The selected events are sorted into different categories depending on their spatial and temporal behavior. Each category of polar arcs is compared to solar wind parameters to find out about a possible correlation between solar wind and arc appearance. Finally, the different polar arc models are compared with the results of this study.

2. Statistics

2.1. Method

[18] For a statistical study of polar arcs in the Northern Hemisphere UV images from the Polar spacecraft are used. The UV imager experiment on Polar provides global images

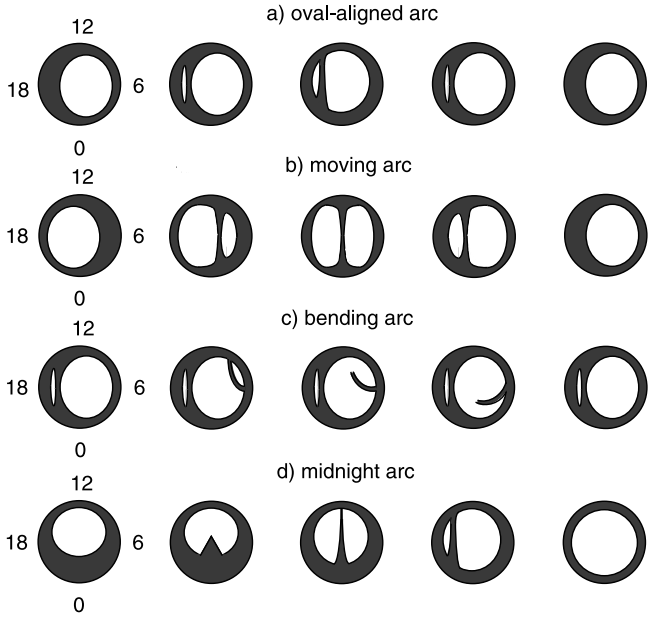

Figure 3. Schematic showing the temporal evolution of all clear polar arc types introduced in the study except multiple arcs.

of the aurora [*Torr et al.*, 1995]. It has an 8-degree field of view and can image the entire auroral oval above 60 degrees geographic latitude at spacecraft altitudes greater than 6 Re. The instrument is able to resolve 0.5 degrees in latitude at apogee; thus a single pixel projected to 100 km altitude from apogee is approximately 50 × 50 km. The study extends over a period of 3 months in winter 1998–1999 (1 December to 28 February). We choose winter months as summer UV images contain too much dayglow to detect the typically faint polar arcs. Sheets of 5 × 6 Polar UV images have been produced with a time interval between each image of at most 6 min. To be able to detect weaker arcs with emission intensities near the instrument threshold UV images are taken with a long integration period (36 s) and a fixed color scale is chosen which shows well the low energy flux range. The scale extends from 0.2 to 20 photons/cm^{2}s. The images are false color images which show the Lyman-Birge-Hopfield molecular nitrogen emissions in the 140–160 nm spectral region. For the image sheets used in this study a linear color scale (with black representing no intensity and white the highest intensity) and the magnetic apex coordinate system [*Richmond*, 1995] with corresponding magnetic local time (MLT) are used. The UVI instrument worked well during the entire 3 months having a high image quality despite two periods (21 December to 4 January and 24–28 February) where the image sensitivity was reduced by about 50% when a transparent MgF window was closed to protect the optics.

2.2. Classification of Polar Arcs

[19] The definition of an event is that an arc is visible in the polar cap or a split oval boundary is seen. Small-scale Sun-aligned arcs do not show up on the UV images because of their low luminosity and limited spatial extent. Polar arcs vary much in scale size, form, and luminosity. For this study, we classify each event as "clear polar arc" or "small split". By small splits we mean arcs which appear for less than 10 min and/or are not separated from the auroral oval clearly enough to allow a distinction from an oval associated arc. Excluded from the study are substorm formations such as extremely deformed substorm current wedges which resemble oval-aligned arcs or auroral streamers (north-south aligned structures within the oval during the recovery phase). Clear polar arcs have a variety of different forms. In the statistical study we found clear polar arcs that either separate from one side of the oval or develop from the nightside oval. Those which separate from the dawnside or duskside oval stay oval-aligned or move poleward. Of the poleward-moving arcs it is possible to distinguish between different subgroups. It also may happen that several different arc types are seen during the same event. A diversity of names exists in the literature to define different forms of polar arcs, but it remains unclear if the names refer to different arc types or only different appearances of the same auroral phenomenon. To avoid any confusion we use our own classification and subdivide the clear polar arcs on the basis of their spatial behavior into five different categories. Figure 3 shows schematically the evolution of each of the first four categories listed below.

1. "Oval-aligned arcs" usually appear near the dawnside or duskside oval but sometimes they may be quite separated from the side of the oval. They do not move considerably before they disappear (Figure 3a).

2. "Moving arcs" refer to those transpolar arcs which move across the entire polar cap unless they fade before reaching the other side of the oval. Moving arcs are not always Sun-aligned; however, both their dayside and nightside oval connection points move (Figure 3b).

3. "Bending arcs" are hook-shaped poleward-moving arcs where the sunward end of the arc separates from the main oval and moves toward the other side of the oval whereas the anti-sunward end remains fixed. An oval-aligned arc is often seen simultaneously on the other side of the oval as indicated in Figure 3c.

4. "Midnight arcs" represent those polar arc events where one single arc develops at the nightside auroral oval from a triangle-like bulge and then stretches toward noon where it may reach to the dayside auroral oval. Before disappearing the arc usually moves toward one side of the oval (Figure 3d).

5. With "multiple arcs" we describe events where many arcs fill the polar cap. There are a multitude of different evolutions, arcs appear simultaneously or one after the other, splitting from an oval side or shooting up from the nightside oval.

All polar arcs found on the UV images during the 3-month period are sorted into one of the above mentioned groups. With the division between small splits and clear polar arcs only the latter unambiguous cases are included in the different arc categories. The start and lifetime of polar arcs are defined by the time the arc is clearly separated from the auroral oval and by the time span from this separation until the arc disappears on the image or reunites with the main oval.

2.3. Comparison With Solar Wind Parameters

[20] To study the influence of solar wind parameters on the occurrence and dynamics of polar arcs we compare the

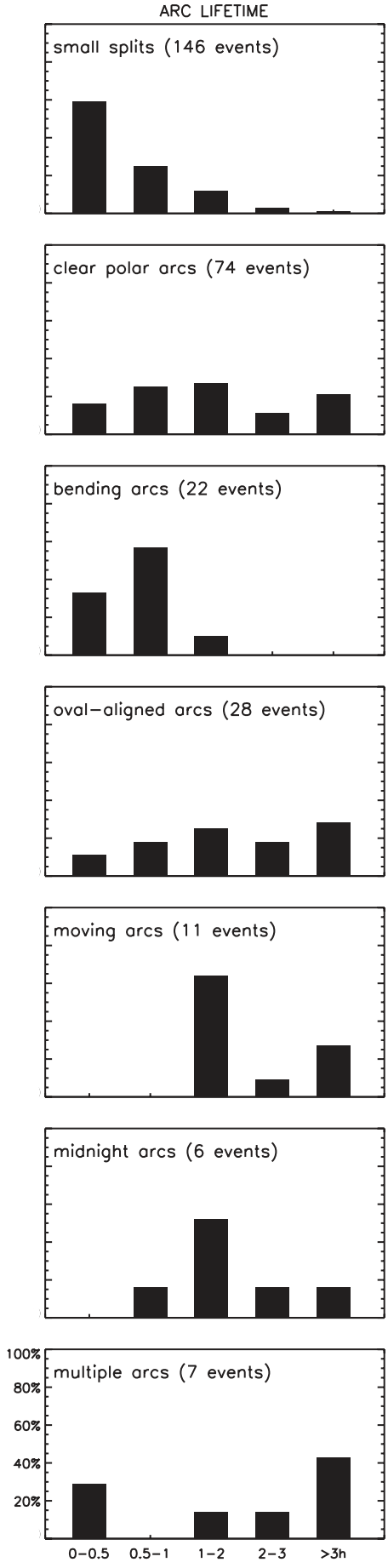

polar arc events with the IMF, solar wind speed, and ion density. For the comparison we use 5-min averaged data from the ACE satellite using GSM coordinates. ACE is located at $\sim$220 R_E sunward of the Earth, and thus the solar wind conditions may have changed slightly when they reach the magnetopause. But since ACE has a nearly continuous coverage of the solar wind it is the most suitable satellite to use for this study. The solar wind data are shifted in time to take into account the propagation time of the solar wind to reach the dayside magnetopause (assumed to be located 10 R_E sunward of the Earth). The time delay is calculated for each day using 24-hour averaged solar wind speed and ACE to Earth magnetopause distance.

3. Results

[21] From the UVI database, 238 different polar arc events have been identified, 92 of which are clear polar arcs and 146 are small splits. For 18 of the clear polar arcs the evolution is not known, because of an insufficient field of view or because of weak emissions near the instrument threshold. These ''unclassified clear polar arc events'' are excluded from further analysis unless explicitly mentioned. The remaining 74 events are grouped into 28 oval-aligned arcs, 22 bending arcs, 11 moving arcs, 6 midnight arcs, and 7 multiple arc events.

3.1. Occurrence Frequency and Lifetimes of Polar Arcs

[22] Only a lower limit of the occurrence frequency of polar arcs can be obtained from the UV images. Approximately 25% of the time the UV imager does not point toward the Earth. These time periods (approximately 4 hours out of the 18-hour orbit period) are excluded from the analysis. The remaining time the imager did not always give a complete enough view of the auroral ionosphere for all polar arcs to be detected. With these limitations in mind we find that clear polar arcs are present during at least 10% of the time and small splits are present at least 6% of the time UV images are available.

[23] Figure 4 shows the lifetimes of small splits, of clear polar arcs, and of all five subtypes of clear polar arcs. The distribution of arc lifetimes as percentages of the events is shown for five time ranges. Only a lower limit of the average lifetime can be given since for 22% of the events the arc begins to develop before it is seen by the UV imager and for 30% of the events the arc disappears from the field of view before it fades. The majority of these events belongs to the category of oval-aligned arcs.

[24] The first two plots in Figure 4 show that a majority of the small splits have lifetimes less than half an hour whereas those of clear polar arcs range from several tens of minutes up to many hours. The plots of the different clear polar arc types show that there exists a characteristic range of lifetimes for most arc types. Bending arcs are nearly as short-lived as small splits whereas moving arcs may last several hours. Oval-aligned arcs seem to have no typical lifetime. Some events last only 30 to 60 min, others may last

Figure 4. (opposite) The distribution of the arc lifetimes as percentages of events for all small splits, clear polar arcs, and each of the clear polar arc types.

several hours. The subsets of midnight and multiple arcs are too small to be treated in a statistical way. For completeness, the study is, however, extended to include even these cases although the results should be treated with care. It can be seen that both midnight and multiple arcs have a large range of lifetimes comparable to those of oval-aligned arcs.

3.2. Spatial Evolution of the Different Polar Arc Types

[25] Figure 5 contains UV images of five clear polar arc events. The UV images in the figure are produced in the same way as the image sheets on which the statistics is based, using an integration period of 36 s and a color scale extending from 0.2 to 20 photons/cm^2 s. Each row in Figure 5 gives an example of the temporal evolution of each arc type. From top to bottom are shown an oval-aligned, a moving, a bending, a midnight, and a multiple arc event. The IMF data corresponding to the examples of different polar arc types shown in Figure 5 is presented in a later section (as Figure 10) where the IMF dependence of polar arcs is evaluated in detail.

[26] It is difficult to define an exact start time for most oval-aligned arcs (see the oval-aligned arc example in Figure 5). They often develop smoothly within an hour from an extension of the dawn or dusk sector oval to a clearly separated arc. In these cases the oval sector is often broad and/or contains multiple parallel bands of discrete arcs within it. More than half of the oval-aligned arcs occur during conditions of very low auroral luminosity of the entire oval. In seven cases it is hard to determine the evolution of the arc as the extremely faint nonmoving arc is visible only for 1 to 2 hours near the polar cap center until it becomes too faint to be detectable. The remaining oval-aligned arcs are clearly visible and all occur at the end of a substorm recovery phase. At least four oval-aligned arcs develop from a double-oval like structure which is a typical feature seen during a substorm recovery phase. Unfortunately, for a majority of the oval-aligned arc events the auroral luminosity is too weak or the imager coverage of the oval insufficient to see both sides of the auroral oval. Still, during at least six events, a secondary, often small or faint arc appears for a short time on the other side of the oval. For those two-thirds of the cases where the fading of an oval-aligned arc is seen by UVI, the arc moves back slightly toward the side of the oval before it disappears. In one-third of the cases a substorm begins while the arc remains visible for up to 1 or 2 hours.

[27] There are five moving arc events where an arc moves across the entire polar cap from one side of the oval to the other (see Figure 5, row 2), in one of the cases the arc moves back to the noon-midnight meridian where it disappears out of the field of view of the imager. In two cases the arcs fade in the center of the polar cap but one of them is such a faint event that it cannot be excluded that this arc reaches the other side of the oval as well. For the remaining cases the start or stop times are uncertain as the arc leaves the field of view before (2 cases) or after (2 cases) the arc reaches the central polar cap. Most of the moving arcs do not consist of only one clear Sun-aligned arc. In four cases the main arc splits into branches. Also, for most events the entire arc is not continuously visible and sometimes a part of the arc disappears. One-third of the moving arc events include a secondary, small arc on the opposite side of the oval. This secondary arc usually appears after the first arc has moved considerably poleward (see the moving arc example in Figure 5). Most of the moving arc events occur during nonsubstorm times. Three moving arcs fade several tens of minutes after a substorm onset.

[28] Bending arcs separate from the oval within 5 to 10 min and start almost immediately to bend into the polar cap where they disappear soon after. Unlike the event presented in Figure 5, row 3 the majority of the bending arcs are very faint and hard to detect on the UV images. Half of the bending arcs are accompanied by an oval-aligned arc on the other side of the auroral oval. In most cases this secondary arc appears before and lasts longer than the very short-lived bending arc. Nearly half of the bending arcs appear during substorm activity.

[29] All but one of the midnight arcs found in this study have a similar evolution. One typical example is shown in Figure 5, row 4. They all occur at the very end of a long substorm recovery phase or possibly at the end of a steady magnetospheric convection period. During the late recovery phase, bulges may appear one after the other at the very active poleward boundary of the nightside oval. In very few cases one of the bulges stretches to extremely high latitudes changing into a triangle-like shape. Out of this triangle a midnight arc shoots toward noon either immediately or up to 40 min later. The arc reaches the noon part of the auroral oval after only 10–20 min. During this process, the extremely broad and contracted main oval returns to normal thickness and size. Afterward, the often irregular midnight arc remains as an oval-aligned like arc for several hours before it fades. Only one of the midnight arcs develops at midnight, the others occur near one side of the oval but with a clear development from a bulge at the nightside auroral oval.

[30] For the multiple arcs, the events differ much from each other. For all events the evolution is very complex and at least one, often faint arc occurs in the middle of the polar cap (like in the example in Figure 5, row 5). In most cases the whole polar cap is filled by many branches. All but one event consist of three or more arcs.

[31] Although for most of the clear polar arcs the division into the five groups described above is obvious, 25% of the 74 clear polar arc events might have been put into a different category. As already mentioned, in seven of the oval-aligned arc cases the evolution is unclear as an arc is only visible for about an hour in the middle of the polar cap. There are 4 hybrid cases between oval-aligned and moving arcs. They are sorted into the group of moving arcs as a slow arc motion toward the central polar cap can be detected. Of the bending arcs, five cases have a nontypical evolution, four of which are very bright and appear at the beginning of a substorm recovery phase, the last consists of a bending arc which later transforms into an oval-aligned arc type. Of the midnight arcs only one event deviates from the typical evolution. It could have been sorted into the group of oval-aligned arcs since no bulge formation is seen before its appearance. For a few oval-aligned arcs and for most of the moving arcs crossing the entire polar cap it cannot be decided whether the arc develops from an existing bulge near one side of the oval similar to a midnight arc or whether the arc separates smoothly from the side of the oval.

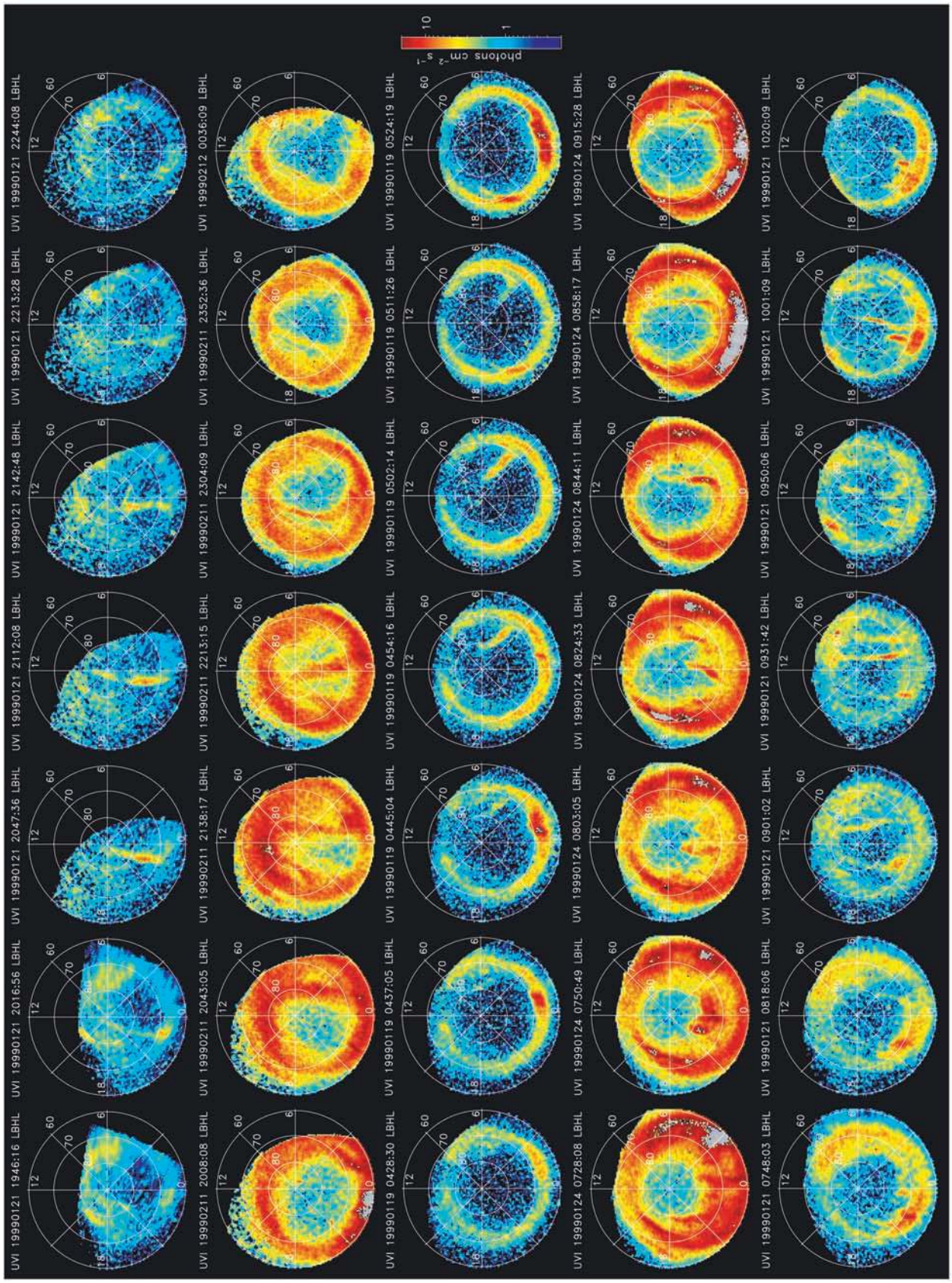
photons cm^{-2} s^{-1}
10
1
UVI 19990121 1946:16 LBHL
UVI 19990121 2016:56 LBHL
UVI 19990121 2047:36 LBHL
UVI 19990121 2112:08 LBHL
UVI 19990121 2142:48 LBHL
UVI 19990121 2213:28 LBHL
UVI 19990121 2244:08 LBHL
UVI 19990211 2008:08 LBHL
UVI 19990211 2043:05 LBHL
UVI 19990211 2138:17 LBHL
UVI 19990211 2213:15 LBHL
UVI 19990211 2304:09 LBHL
UVI 19990211 2352:36 LBHL
UVI 19990212 0036:09 LBHL
UVI 19990119 0428:30 LBHL
UVI 19990119 0437:05 LBHL
UVI 19990119 0445:04 LBHL
UVI 19990119 0454:16 LBHL
UVI 19990119 0502:14 LBHL
UVI 19990119 0511:26 LBHL
UVI 19990119 0524:19 LBHL
UVI 19990124 0728:08 LBHL
UVI 19990124 0750:49 LBHL
UVI 19990124 0803:05 LBHL
UVI 19990124 0824:33 LBHL
UVI 19990124 0844:11 LBHL
UVI 19990124 0858:17 LBHL
UVI 19990124 0915:28 LBHL
UVI 19990121 0748:03 LBHL
UVI 19990121 0818:06 LBHL
UVI 19990121 0901:02 LBHL
UVI 19990121 0931:42 LBHL
UVI 19990121 0950:06 LBHL
UVI 19990121 1001:09 LBHL
UVI 19990121 1020:09 LBHL

[32] Since the small split category contains all ambiguous cases it includes a multitude of different types. For completeness we mention them briefly: There exist oval-aligned arc-like splits which may be part of the main oval (35 events) and splits which occur at the end of a double oval event where the poleward oval boundary connects to the nightside such that an oval-aligned arc-like structure appears (13 events). Many other splits resemble bending arcs but with a very short length and lifetime. They appear near noon (24 events) or near the nightside oval (9 events). Another group consists of arcs which are clearly separated from the oval but with such low luminosity that one cannot decide if it is a polar arc or not (18 events). Midnight arc type splits are extremely large triangles which extend from the nightside to very high latitudes but do not develop into an arc which stretches further than the dawn-dusk meridian (32 events). Splits related to substorms are often arcs which may be part of an extremely expanded auroral bulge (15 events).

3.3. Comparison With Solar Wind Data

[33] In Figure 6 an overview time-sequence plot of all 3 months is shown with all polar arc events overlaid on solar wind data (light grey for small splits, dark grey for clear polar arcs including unclassified clear polar arc events). The first four rows show the total magnitude of the IMF, the IMF B_z component, the solar wind density, and the solar wind velocity measured by the ACE satellite. The IMF B_z component overlaid with polar arc events demonstrates the well-known fact that polar arcs preferably occur for northward IMF and disappear completely during long periods of southward IMF B_z (e.g., 10–11 December, 27 January, or 19 February). Large-scale fluctuations of the solar wind velocity and density seem not to be connected to the occurrence probability of polar arcs but the IMF magnitude is usually higher during periods with a high frequency of polar arcs. However, during periods of a very high occurrence frequency of polar arcs, such as 1–3 December or 20–22 January, the solar wind speed is higher than average. By combining the IMF magnitude with solar wind speed and the cosine function of the IMF clock angle θ (giving high values for northward IMF as $\theta = \arctan(|B_y|/B_z)$ for B_z>O and $\theta = \pi \arctan(|B_y|/B_z)$ for B_z<O in the following form $vB^2 \cos^4(\theta/2)(l_0^2/\mu_0)$ a parameter is obtained which correlates better with the occurrence probability of polar arcs than any of the solar wind parameters on their own. This parameter, which we refer to as the *anti-epsilon* parameter has the same form as the Akasofu-Perreault epsilon parameter [*Perreault and Akasofu*, 1978] but with a cosine function replacing the sine function. The factor l_0^2/μ_0 (with $l_0 = 7R_E$) is included in the anti-epsilon parameter to make the form similar to the epsilon parameter. By definition the anti-epsilon parameter has values near zero for strong southward IMF. During periods where the IMF is mainly northward but no polar arcs occur (e.g., 1–2 and 6–8 February) the parameter decreases to very low values as well. The peak values of the parameter overlap with long-lived arcs and/or a high polar arc density. However, there are certain days (e.g., 27 December or 26 February) with a lack of polar arc events despite quite a high magnitude of the anti-epsilon parameter. These days belong to the periods where the transparent MgF window was closed. Because of the low image resolution faint polar arc events have probably been missed. The anti-epsilon parameter and its correlation with polar arc occurrence will be discussed below in more detail.

[34] To be able to study the connection between arc occurrence and solar wind data in more detail the hourly averaged solar wind values before, during, and after the polar arc events are examined. The results are presented in Figures 7, 8, 11, and 12. These figures show the distribution of the IMF, the solar wind speed, density, dynamic pressure, energy flux, and the anti-epsilon parameter for all detected polar arcs. The plots are all done in a similar way. The values of each solar wind parameter are divided into four intervals. The range of each interval is chosen such that the solar wind parameter has values within one interval during 25% of the time. The time covered by the statistics includes the entire 3-month period except for the time intervals for which the UV imager did not point toward the auroral oval. Each of the plots show 12 different distributions given as percentages of polar arc events, the hourly averaged distribution up to 5 hours before and after the events (grey bars to the left and the right of the black bars) the distribution at the event start (left black bar) and the distribution of the average value during the event (right black bar). With these plots it is possible to get information not only on the typical distribution of the solar wind parameters for each type of polar arc event but also of the development of the solar wind values before, during, and after the events. Binning the solar wind data into four equal intervals makes any deviation from the average solar wind distribution more readily visible.

3.4. Connection Between Polar Arcs and Hourly Averaged IMF Components

[35] In Figure 7 the distribution between positive and negative signs of each IMF component are shown for each polar arc type. Here the above described grey and black bars are ordered from top to bottom, beginning with the average distribution for the 5th hour before the event at the top and ending with the 5th hour after the event at the bottom. The left and right dotted lines of each panel show the percentage of time (covered by the statistics) the IMF B_x, B_y, and B_z components have negative and positive values, respectively. Figures 8a–8c consist of distribution plots as described above for each of the IMF components IMF B_x, B_y, and B_z.

[36] The dotted lines in Figure 7 show that during the time period of the statistics, negative IMF B_x and positive B_y are dominant while B_z is equally distributed between both signs. This corresponds to the most common solar wind distribution. Comparing the distribution of the IMF components for small splits with those of the clear polar arcs (first two rows in Figures 7 and 8), it seems that the IMF B_x and

Figure 5. (opposite) Examples of clear polar arcs seen on the Polar UV imager. Each row shows the temporal evolution (from left to right) of one clear polar arc event (from top to bottom): Oval-aligned arc, moving arc, bending arc, midnight arc, and multiple arc event.

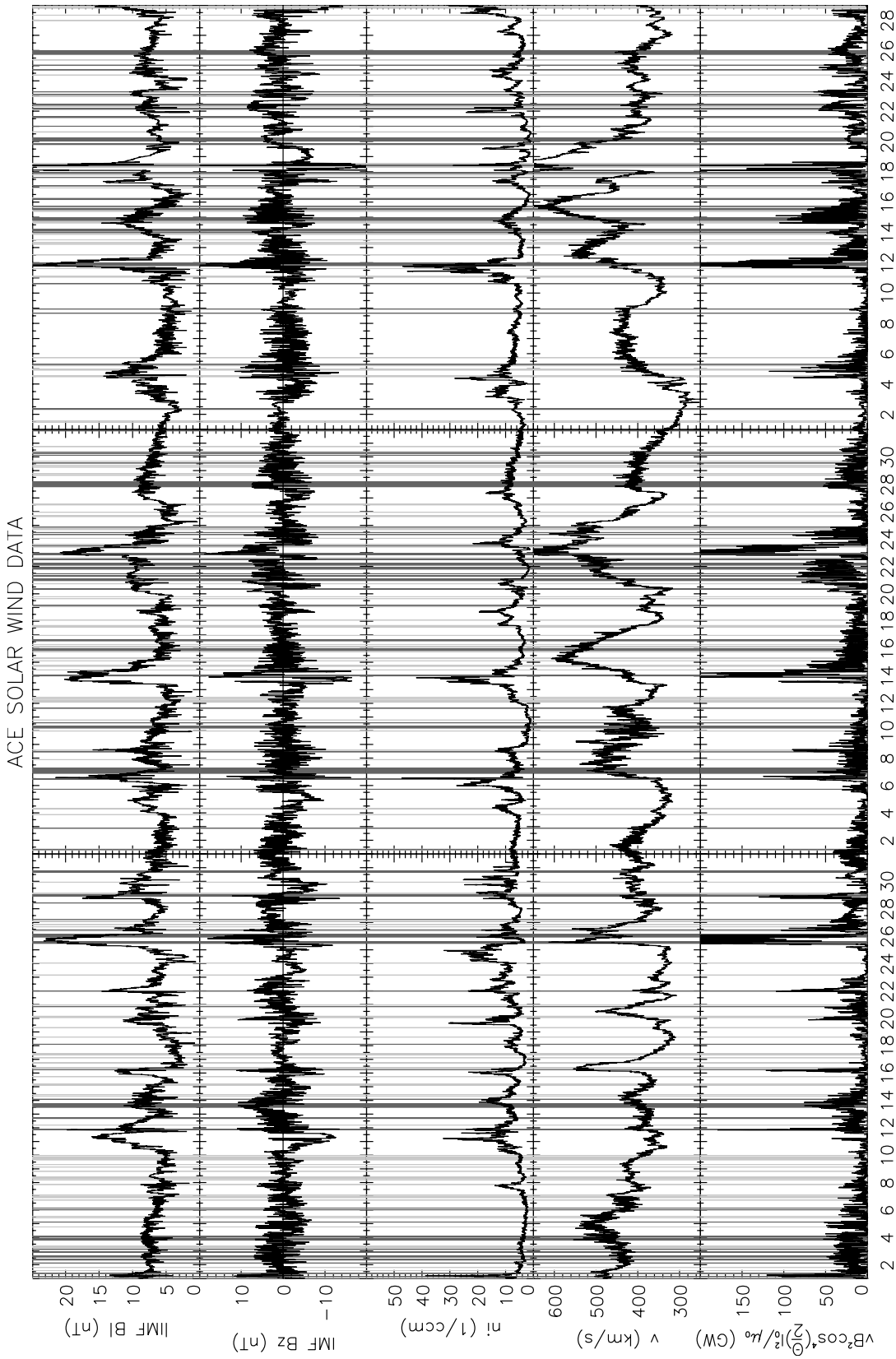

Figure 6. Overview plot of the entire statistical period with all polar arc events found in the Polar UV images overlaid on ACE solar wind data. From top to bottom, the total IMF magnitude, the IMF B_z component, the solar wind density, the solar wind velocity, and the anti-epsilon parameter are shown. The light grey and dark grey bars correspond to small splits and clear polar arc events, respectively.

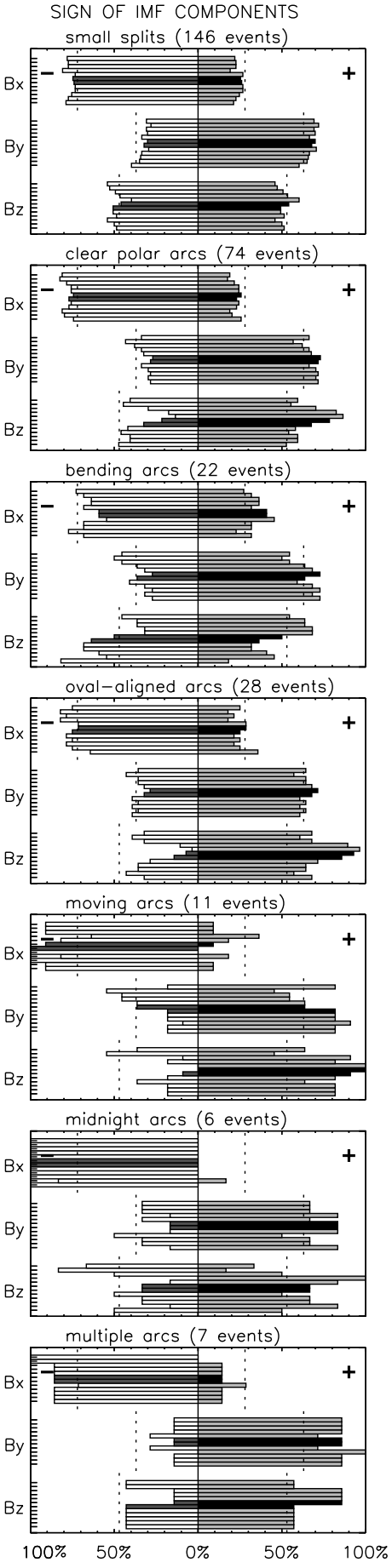

Figure 7. (opposite) The distribution of the sign of each IMF component as percentages of events for all small splits, clear polar arcs, and each of the clear polar arc types. The dotted lines give the distribution between positive and negative signs of each IMF component during the statistical time period. The grey bars above (below) the black bars show the hourly averaged IMF component signs up to 5 hours before (after) the polar arc event. The first and second black bars show the IMF component sign at the event start and the average IMF component sign during the event.

B_y distributions are similar to the average IMF distribution during the statistical time period and they do not change much during the 10 hours around the event. For the IMF B_z component, though, a clear difference between small splits and clear polar arcs is found. Small splits occur for weak IMF B_z with as many southward IMF as northward IMF cases. Clear polar arcs show a strong preference for northward IMF conditions. The highest percentage of northward IMF is found 1 to 2 hours before the event start. During the event the IMF is still northward for the majority of cases but already the hour after the event an average IMF B_z distribution is found.

[37] Looking at the different clear arc types (last five rows in Figures 7 and 8), major differences in the IMF distributions are found between bending, oval-aligned, and moving arcs. Midnight and multiple arcs have IMF characteristics similar to those of the moving arcs. The IMF B_x distribution shown in Figure 7 for bending and oval-aligned arcs is similar to the IMF B_x distribution itself. Bending arcs occur slightly more often for positive, oval-aligned arcs slightly more often for negative IMF B_x, compared to the average IMF B_x distribution during the statistical time period. In contrast to this, the last three arc types have a clear preference for negative IMF B_x. From Figure 8a it can be seen that for these arc types IMF B_x is not only negative but strongly negative. Most of the events occur for IMF B_x less than -5.4 nT, nearly none of them has positive IMF B_x values greater than 0.5 nT. The distribution of the IMF B_y component is less clear (Figures 7 and 8b). Bending and oval-aligned arcs occur for an average IMF B_y distribution, moving arcs mainly for weak IMF B_y, most often negative before and positive after the events, most midnight and multiple arcs occur during positive IMF B_y. The most significant difference between the clear polar arc types is found for the IMF B_z distribution (Figure 7). While bending arcs start to develop as often for B_z positive as negative, oval-aligned and moving arcs occur almost exclusively during northward IMF. Most midnight and multiple arcs develop during northward IMF. The change of the IMF B_z sign distribution in time is, however, similar for all clear polar arc events. The highest (lowest) number of northward IMF cases is found 1 to 2 hours before (after) the events. Looking at the strength of IMF B_z in Figure 8c, it is interesting that some bending arcs occur for IMF B_z values less than -2.3 nT while all other arc types appear during positive or only weakly negative IMF B_z values.

[38] As could be expected from earlier studies, a strong dependence is found of the polar arc location on the sign of IMF B_y. These results are presented in Table 1, listing the number of arcs which at their start time appear on the

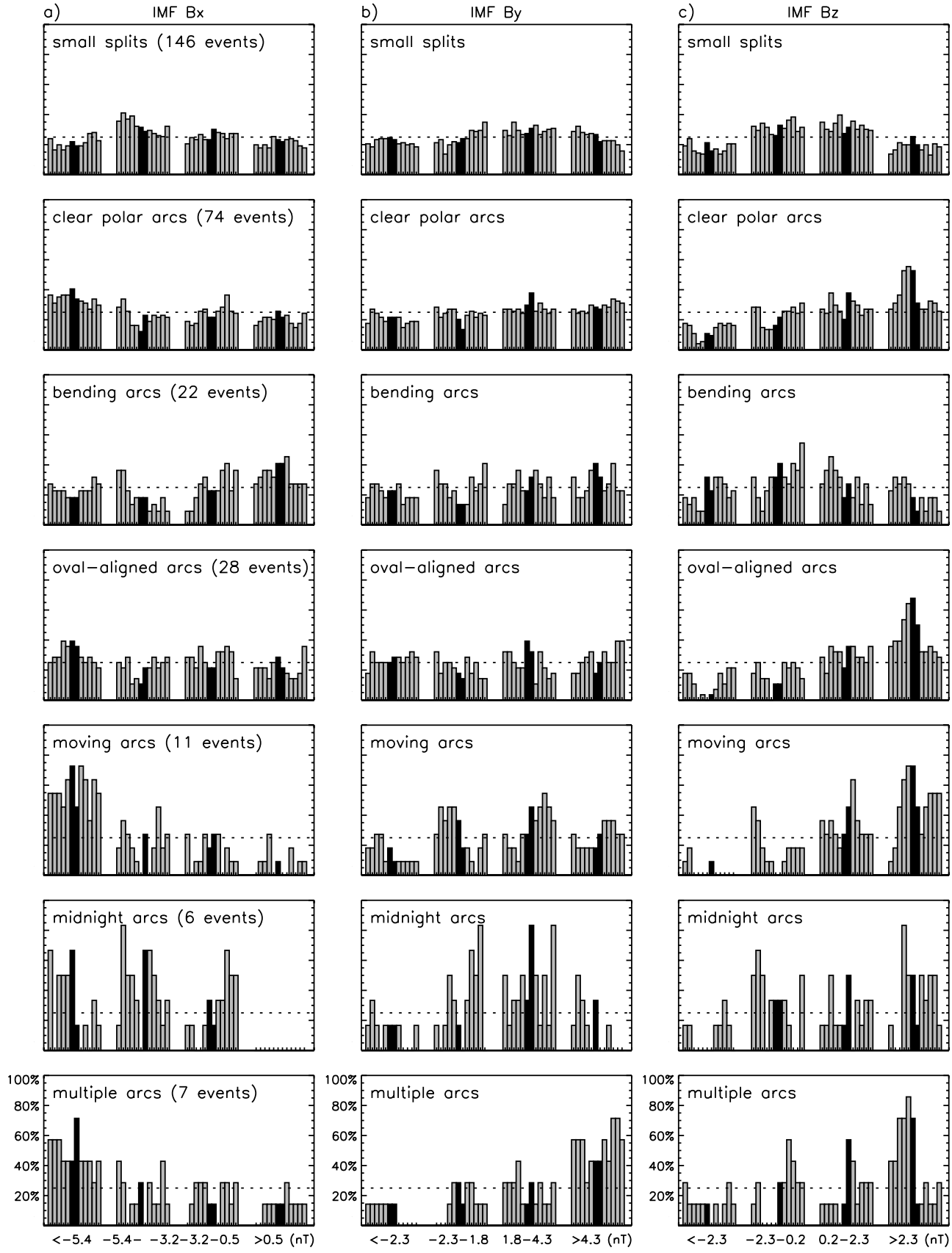
a)
IMF Bx
b)
IMF By
c)
IMF Bz
small splits (146 events)
small splits
small splits
clear polar arcs (74 events)
clear polar arcs
clear polar arcs
bending arcs (22 events)
bending arcs
bending arcs
oval−aligned arcs (28 events)
oval−aligned arcs
oval−aligned arcs
moving arcs (11 events)
moving arcs
moving arcs
midnight arcs (6 events)
midnight arcs
midnight arcs
multiple arcs (7 events)
multiple arcs
multiple arcs
100%
80%
60%
40%
20%
<−5.4
−5.4− −3.2
−3.2−0.5
>0.5 (nT)
<−2.3
−2.3−1.8
1.8−4.3
>4.3 (nT)
<−2.3
−2.3−0.2
0.2−2.3
>2.3 (nT)

Table 1. Polar Arc Locations at Their Start Time Versus Average IMF B_y Values During the Events

	Duskside Arc		Middle Arc		Dawnside Arc	
Arc Type	$B_y > 0$	$B_y < 0$	$B_y > 0$	$B_y < 0$	$B_y > 0$	$B_y < 0$
small splits	43	17	27	6	32	21
clear polar arcs	24	8	6	0	23	13
bending arcs	1	5	0	0	13	3
oval-aligned arcs	14	1	3	0	2	8
moving arcs	2	2	1	0	6	0
midnight arcs	3	0	1	0	1	1
multiple arcs	4	0	1	0	1	1

dawnside, in the middle, or on the duskside of the oval sorted by the average sign of IMF B_y during each event.

[39] Interestingly, there is only a marginal difference between the number of dawnside and duskside polar arcs. The majority of small splits and clear polar arcs appear during positive IMF B_y. This is probably due to the fact that IMF B_y is positive during two-thirds of the statistical time period. From Table 1 it is clear that most bending and moving arcs start to develop at the side of the oval which is opposite to the direction of the IMF B_y component. Both arc types move poleward, which means that most of these arcs move in the direction of IMF B_y. The nonmoving arc types, midnight and oval-aligned arcs, are on average located at the side of the oval toward which the IMF B_y component points. Also, multiple arc events start with an arc which appears at the side of the oval in direction of IMF B_y. Looking at the sign of IMF B_y at the event start time instead of the average during the event shows the same tendency, slightly better for bending arcs but less clear for oval-aligned and moving arcs.

[40] Each arc type contains 10–20% of cases which deviate from this scheme. Several of them are hybrid or faint events. Other clear polar arcs develop during IMF conditions which only slightly deviate from the expected IMF behavior. This includes cases such as an oval-aligned arc which occurs for IMF B_y having the "wrong" sign but values close to zero or a moving arc which appears after a clear IMF B_y drop from positive to zero instead of a sign change. Only the location of one midnight arc deviates clearly from the expected pattern. Not included in Table 1 are the secondary arcs which develop during one-third of all clear polar arc events. They are often very small or faint such that most of them could be categorized as small splits. Nearly all secondary arcs occur for the same IMF B_y sign (taking the average IMF B_y during the lifetime of the second arc) as the main arc itself.

3.5. Connection Between Polar Arcs and IMF Sign Changes

[41] Very interesting results are found from looking at the clock angle distributions for the different polar arc types in Figure 9. In this figure, the IMF clock angles between IMF B_z and the absolute value of IMF B_y are shown. The clock angles ranging from 0 (pure northward IMF) to 180 degrees (pure southward IMF) are divided into five equally large intervals. Each row shows for each polar arc type the average clock angle distribution (from left to right) 2 hours before, 1 hour before, at the event start, and during the event. The average IMF distribution during the entire statistical period is shown as the grey shaded areas in the first plot of the top row.

[42] On average, the IMF is distributed equally between positive and negative B_z with $|B_y|$ dominating $|B_z|$ most of the time. Small splits occur preferably for dominating $|B_y|$ and small, positive B_z. As expected already from Figures 8b and 8c the IMF clock angle does not change considerably for small splits. For bending arcs the average IMF clock angle distribution changes from around 70 degrees 1 hour before the event to around 100 degrees at the event start and back to around 80 degrees during the event. This corresponds to an IMF B_z sign change from northward to slightly southward and back again. Oval-aligned arcs occur on average for a constant IMF clock angle distributions around 45 degrees. The average IMF distribution changes toward this IMF clock angle distribution around 1 hour before the event start. Moving arcs occur on average approximately 1 hour after a change from 45 degrees toward strictly northward IMF and back again. As discussed below, this IMF clock angle change is due to an IMF B_y sign change. An IMF B_y sign change cannot be seen in this kind of plot since the absolute value of IMF B_y is used. For midnight and multiple arcs the IMF clock angle changes are less clear, but both occur for varying IMF clock angles during predominantly northward IMF. The IMF clock angle distribution plots of Figure 9 give only the percentage of events with an IMF clock angle within a certain interval. Thus, one cannot conclude with certainty from these plots that an IMF B_z (IMF B_y) sign change takes place for each single bending (moving) arc event or that all oval-aligned arcs occur during constant IMF.

[43] Table 2 gives the percentage of cases which contain IMF B_x, B_y, or B_z sign changes during the last 10 min (left column) and during the last 60 min (right column) before the polar arc starts to appear. In both cases sign changes up to 10 min after the event start have been included because of a possible uncertainty in the arc start time (it is often

Figure 8. (opposite) The distribution of (a) IMF B_x, (b) IMF B_y, and (c) IMF B_z as percentages of events for all small splits, clear polar arcs, and each of the clear polar arc types. The different magnitude ranges are chosen such that the IMF component is equally distributed between the four intervals during the statistical time period (dotted line at 25%). The grey bars to the left (right) of the black bars show the distribution of the hourly averaged IMF component up to 5 hours before (after) the polar arc event. The black bars show the IMF magnitude distribution at the event start (left black bar) and the average IMF magnitude distribution during the event (right black bar).

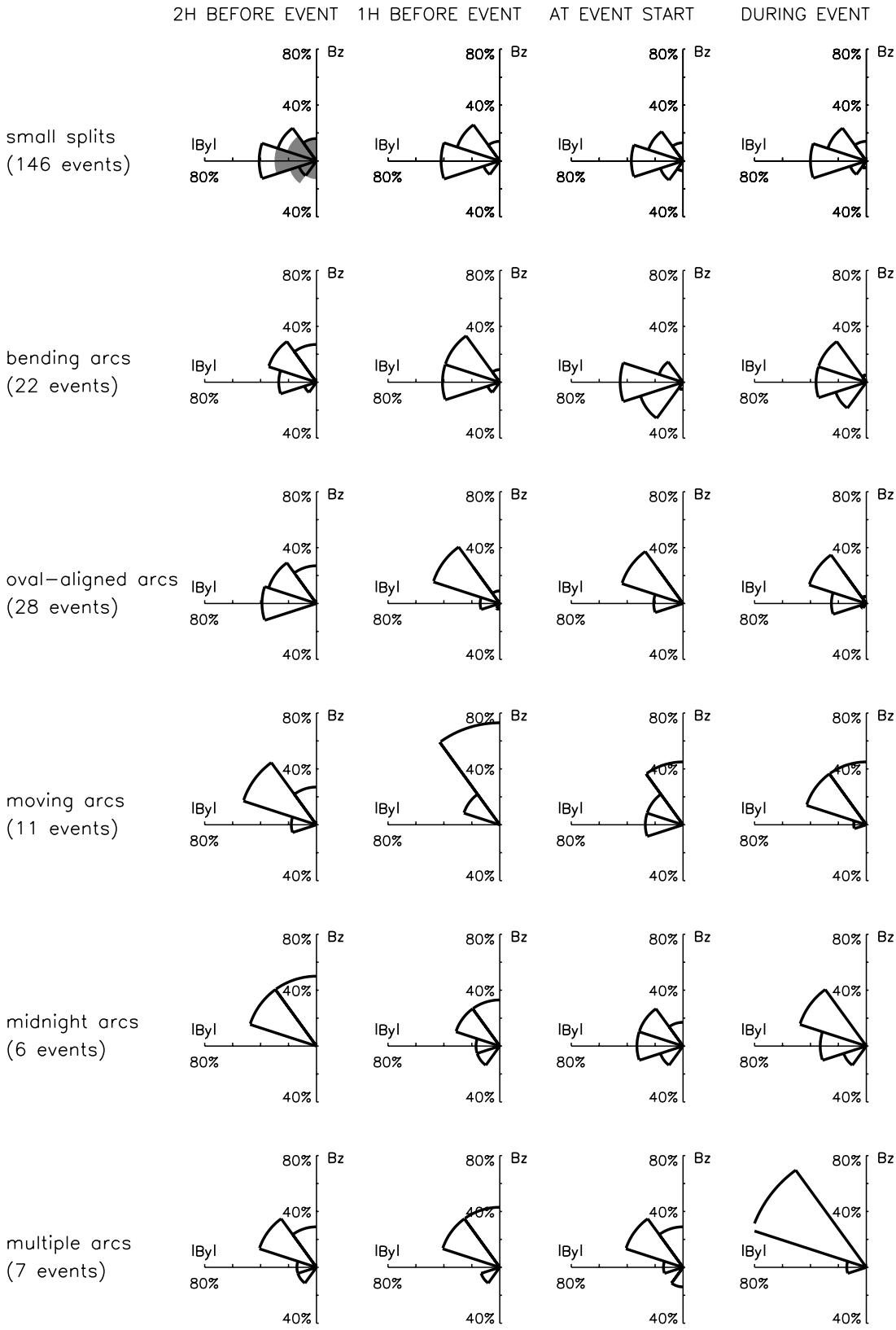

Figure 9. The distribution of the IMF clock angle between IMF B_z and the absolute value of IMF B_y for each polar arc type. The distributions of the hourly averaged clock angles for the second and the first hour before the events, at the event start, and the average value during the events are shown. The grey shaded areas in the first plot of the top row show the average IMF clock-angle distribution during the statistical time period.

Table 2. Percentages of Polar Arc Events With IMF Sign Changes Occurring Within Two Different Time Intervals Around the Arc Start Times

	B_x Sign Change		B_y Sign Change		B_z Sign Change	
Arc Type	−10/+10 min	−60/+10 min	−10/+10 min	−60/+10 min	−10/+10 min	−60/+10 min
small splits	12%	27%	16%	34%	42%	69%
clear polar arcs	8%	31%	14%	39%	34%	57%
bending arcs	5%	32%	9%	23%	50%	82%
oval-aligned arcs	18%	29%	14%	29%	18%	39%
moving arcs	0%	36%	18%	82%	27%	45%
midnight arcs	0%	17%	17%	67%	67%	67%
multiple arcs	0%	43%	14%	43%	29%	57%

difficult to define an exact start time from the UV images and the IMF data used for comparison is 5-min averaged data).

[44] Table 2 shows the same tendency as the IMF clock angle distribution plots. Nearly all of the bending (moving) arcs occur after an IMF B_z (IMF B_y) sign change. For half of the bending arcs an IMF B_z sign change takes place within 10 min of the start time but only one quarter of the moving arcs occur directly before or after an IMF B_y sign change. Most moving arcs start to develop 10 to 60 min after an IMF B_y sign change. Nearly half of the moving arcs involve an IMF B_z sign change as well. Interestingly, many small splits occur in connection with an IMF B_z sign change. Only oval-aligned arcs have a low rate of IMF sign changes. The majority of midnight and moving arcs involve both IMF B_y and IMF B_z sign changes. Except for multiple arcs only a minority of polar arcs appear after an IMF B_x sign change.

[45] Studying IMF time series for each of the clear polar arc events confirms the tendency shown in Table 2. Eight of 11 moving arcs appear after an IMF B_y sign change which took place up to 1 hour before the event start. Of the three other events, two events are hybrid cases which may be classified as oval-aligned arcs, one of them contains an IMF B_y drop from strongly positive to around zero. Only one unclear case exists (it may in fact be a midnight arc) where the arc moves nearly over the entire polar cap, without an IMF B_y sign change taking place within hours. Most bending arcs occur for small values of IMF B_z, changing several times between positive and negative values. All but one bending arc appear after an IMF B_z sign change. This event may be a multiple arc event since a secondary arc appears from midnight. Unfortunately, the field of view does not allow the entire event to be observed. From the comparison between event start and IMF data (which may contain uncertainties up to 10 min) we find that one-third of the bending arcs appear at an IMF B_z southward turn, one-third appear during a southward IMF period approximately 20–30 min after the last or before the next B_z sign change and one-third occur at the B_z sign change back to northward. The negative IMF B_z period is between 20 and 40 min long for half of the cases, for the other half it lasts 1 to 2 hours. Only in one case there is a strong B_z southward period of several hours. The only clear polar arcs which occur after many hours of nearly constant IMF are oval-aligned arcs. Not all oval-aligned arcs appear during these conditions. One-third of the oval-aligned arcs occur after an IMF B_y or B_z sign change, another third involves an IMF B_z or IMF B_y sign change during the event. For midnight and multiple arcs the IMF contains several sign changes. As the data look very different from case to case no clear tendency is found.

[46] Figure 10 shows the IMF data for the five arc-type examples of Figure 5. The plots demonstrate the clock angle dependence of the different arc types discussed in this section. The data is shifted in time to take into account the average distance of ACE to Earth magnetopause and average solar wind velocity during the 6 hours shown in the plots. The grey regions mark the arc lifetime, the dotted (and dashed) lines mark the start and stop times of a secondary arc (and tertiary arc in case of appearance). For the midnight arc event the dotted line indicates the time a triangle-shaped bulge develops. The oval-aligned arc occurs for nearly constant IMF B_y and B_z. The moving arc starts to develop during a major IMF B_y sign change, and a secondary arc appears at an IMF B_z drop to zero. The bending arc appears 15 min after a small IMF B_z southward turn. A midnight arc occurs during changing IMF B_z 35 min after the development of a bulge. The IMF was predominantly northward during the 2 hours preceding the bulge development. The three arcs of the multiple arc event appear during slightly changing IMF B_y and B_z.

3.6. Connection Between Polar Arcs and IMF Magnitude, Solar Wind Velocity, and Density

[47] Figure 11 shows the distribution of the IMF magnitude (Figure 11a), solar wind velocity (Figure 11b), and solar wind density (Figure 11c) for all polar arc events. The plots are done in the same way as the plots for the IMF B_x, B_y, B_z components in Figure 8.

[48] Studying the IMF magnitude distribution in Figure 11a, it is easily seen that small splits have a distribution which is nearly identical with the IMF distribution itself while most clear polar arcs appear for larger IMF values. The values of the IMF magnitude before, during, and after the event are approximately the same. Looking at the different clear polar arc types, bending arcs have a similar distribution as small splits, all other arc types occur on average for higher IMF magnitude. Moving arcs contain the highest percentage of cases which occur during strong IMF.

[49] The distribution plots of the solar wind speed (Figure 11b) show that not only most of the clear polar arcs but also most small splits appear during times of higher solar wind velocities than average. Bending arcs have again a distribution similar to small splits. Only oval-aligned arcs have a nearly average velocity distribution. Most moving, midnight, and multiple arcs occur during times of very high solar wind velocities.

[50] Interestingly, the solar wind density is neither correlated to small splits nor to clear polar arcs (Figure 11c). The density distributions for each clear polar arc type shows no clear tendency. Bending, oval-aligned, and multiple arcs

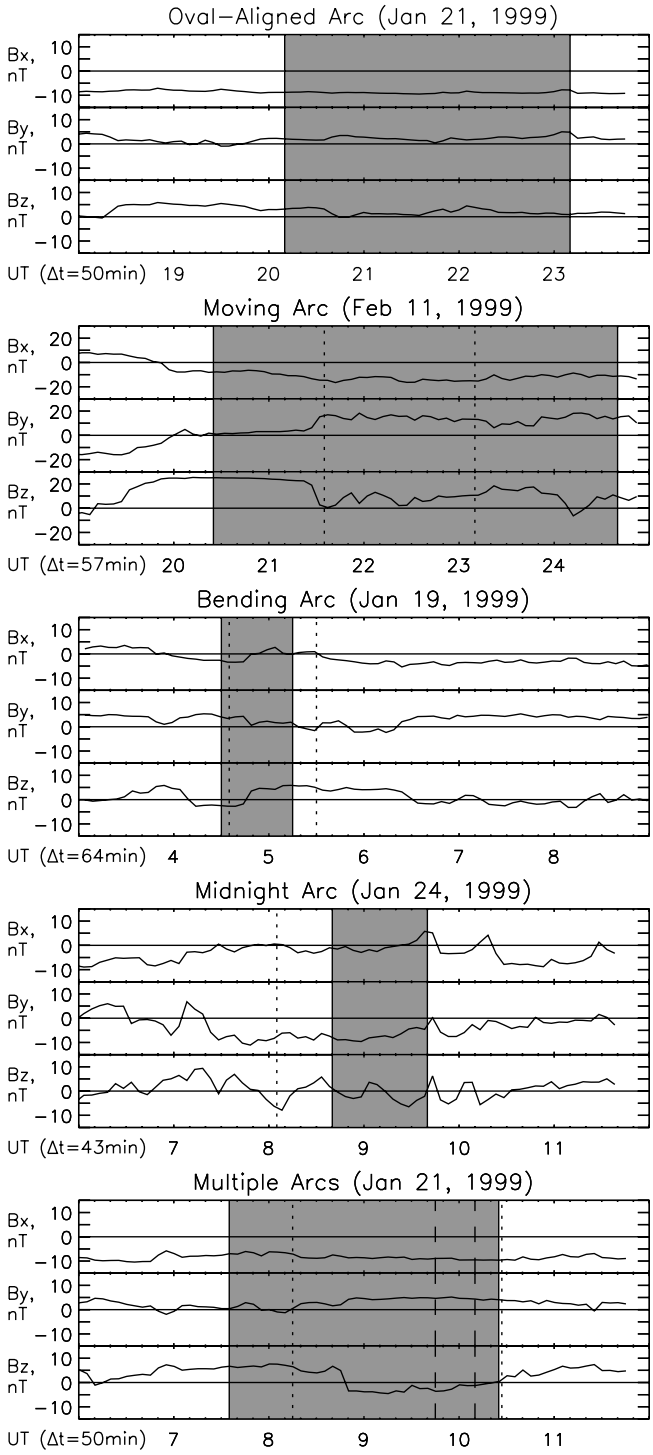

Figure 10. IMF components from ACE data for each of the clear polar arc type examples shown in Figure 5. The propagation time Δt (calculated from a 6-hour average of velocity and distance of ACE to Earth) is added to the time. The grey region shows the time period of the arc occurrence and the dotted lines show (in case of existence) start and stop times of the secondary and tertiary arcs except in the second to last plot, where the dotted line indicates the appearance of a bulge.

correlate with the average density distribution during the statistical time period whereas midnight arcs lack cases with highest density values and moving arcs occur either for very low or very high solar wind densities.

3.7. Connection Between Polar Arcs and Solar Wind Dynamic Pressure, Energy Flux, and the Anti-Epsilon Parameter

[51] In Figure 12, three derived quantities from the basic solar wind parameters are shown, the solar wind dynamic pressure $\rho_i v^2$ (Figure 12a), the solar wind energy flux $(1/\mu_0)vB^2$ (Figure 12b), and the anti-epsilon parameter $(l_0^2/\mu_0)vB^2 \cos^4(\theta/2)$ (Figure 12c) introduced above.

[52] One might expect that the solar wind dynamic pressure plays a role in the occurrence of polar arcs. This is not so obvious as demonstrated in Figure 12a which presents the solar wind dynamic pressure for all polar arcs. Neither small splits nor clear polar arcs deviate much from the average dynamic pressure distribution. Looking at each arc type in detail, one finds that both bending and oval-aligned arcs have average dynamic pressure distributions. For moving arcs the result is unclear, they do not appear within 1.2–2.4 nPa dynamic pressure range. Due to the very high solar wind velocities, midnight and multiple arcs have many cases with high solar wind dynamic pressure. This is most pronounced for midnight arcs with more than half of the events in the highest range of solar wind dynamic pressure.

[53] Looking at the solar wind energy flux $(1/\mu_0)vB^2$ in Figure 12b, one finds, as expected from the IMF magnitude and solar wind velocity distribution plots in Figures 11a and 11b, that the distribution of the energy flux for small splits corresponds to the average distribution during the statistical time period while clear polar arcs often occur for high energy flux values. Again, bending arcs have a nearly average energy flux distribution, oval-aligned arcs dominate only slightly for higher energy flux while the last three arc types occur during solar wind conditions with extremely high energy flux.

[54] The anti-epsilon parameter which combines the effect of strong solar wind velocity, IMF magnitude, and small IMF clock angle results in even more pronounced distributions within the range of high values (Figure 12c). Also small splits appear more frequently for higher anti-epsilon values. Of the clear polar arc events nearly 60% appear for the highest anti-epsilon values. For most clear polar arcs the anti-epsilon value is clearly higher than average during at least 5 hours before and after the events due to the IMF magnitude and the solar wind velocity distributions (comparing Figure 12c with Figures 11a and 11b). As expected from Figures 7, 8b, 8c, 11a, and 11b the distribution of the anti-epsilon parameter is nearly the same before and after the events for small splits whereas for clear polar arcs the anti-epsilon distribution changes considerably. The number of clear polar arc cases with highest anti-epsilon values increases to a maximum 2 hours before the start time and decreases to lower values during the event. The main cause for this is the change of the IMF B_z distribution with time (Figure 8c). The anti-epsilon distribution plots for each type of clear polar arcs reveal that all except bending arcs occur mostly for highest anti-epsilon values and have similar time-histories of the anti-epsilon

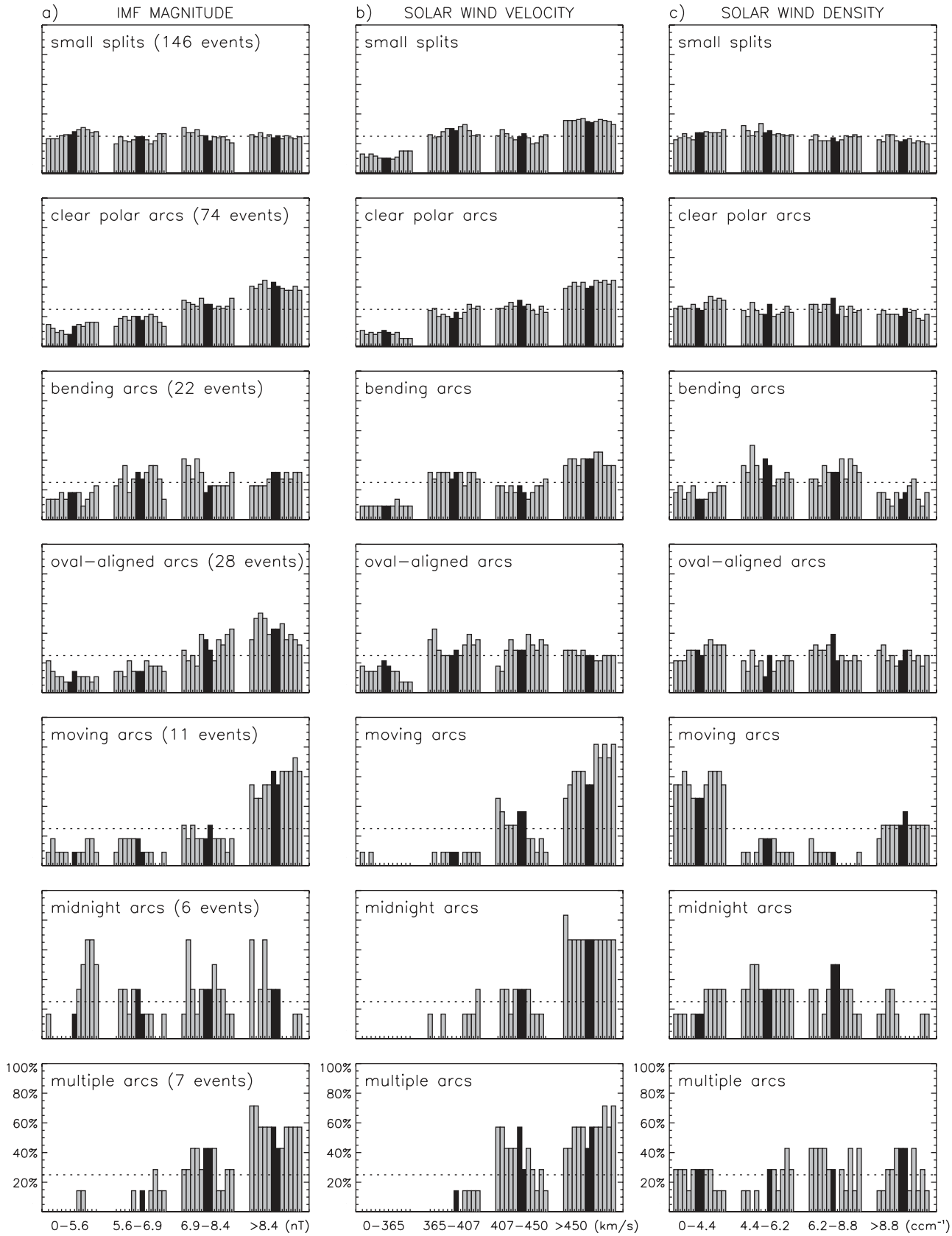

Figure 11. The distribution of (a) IMF magnitude, (b) solar wind velocity, and (c) solar wind density as percentages of polar arc events. The figures are done in the same way as Figure 8.

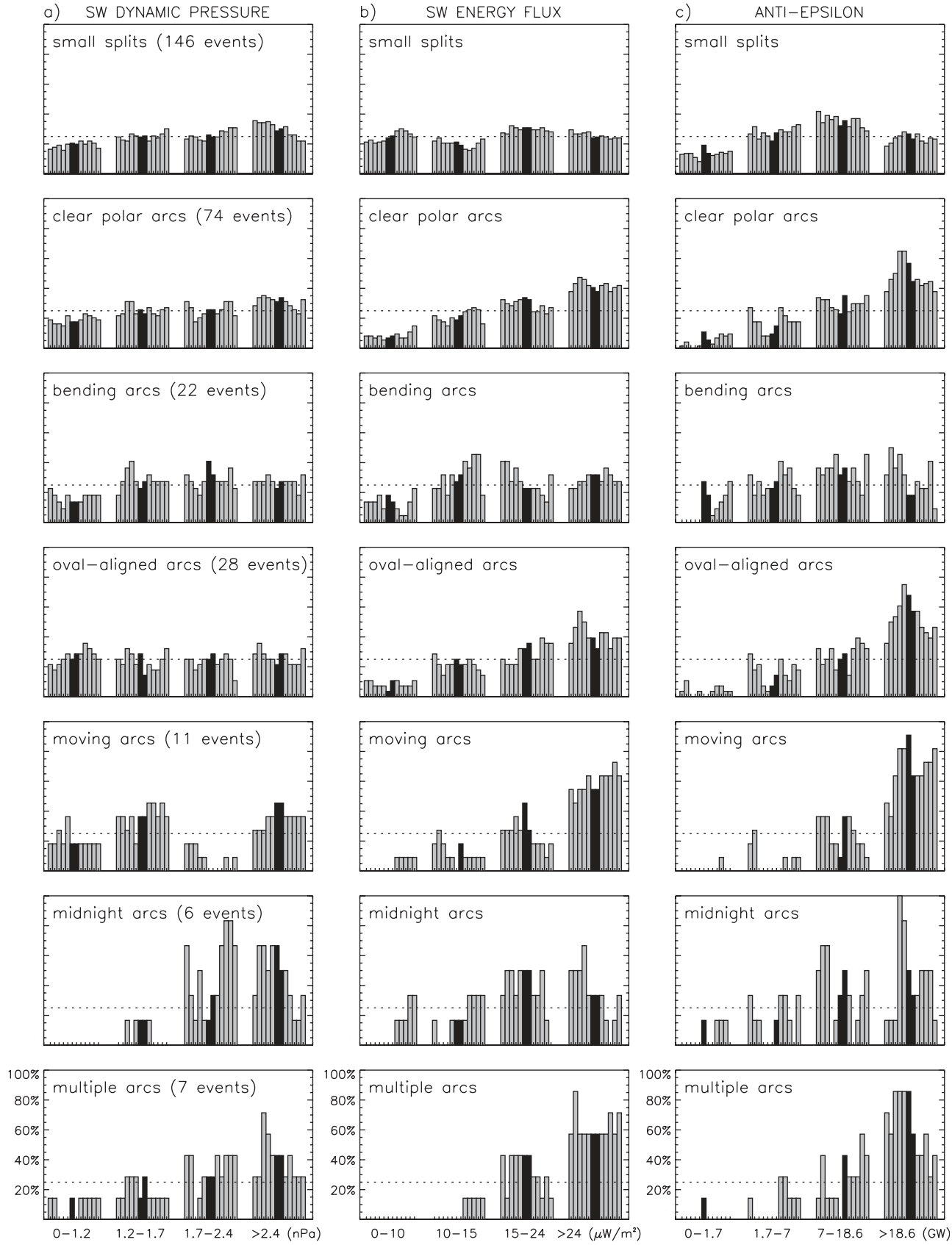
a) SW DYNAMIC PRESSURE
b) SW ENERGY FLUX
c) ANTI−EPSILON
small splits (146 events)
small splits
small splits
clear polar arcs (74 events)
clear polar arcs
clear polar arcs
bending arcs (22 events)
bending arcs
bending arcs
oval−aligned arcs (28 events)
oval−aligned arcs
oval−aligned arcs
moving arcs (11 events)
moving arcs
moving arcs
midnight arcs (6 events)
midnight arcs
midnight arcs
multiple arcs (7 events)
multiple arcs
multiple arcs
100%
80%
60%
40%
20%
0−1.2
1.2−1.7
1.7−2.4
>2.4 (nPa)
0−10
10−15
15−24
>24 (μW/m²)
0−1.7
1.7−7
7−18.6
>18.6 (GW)

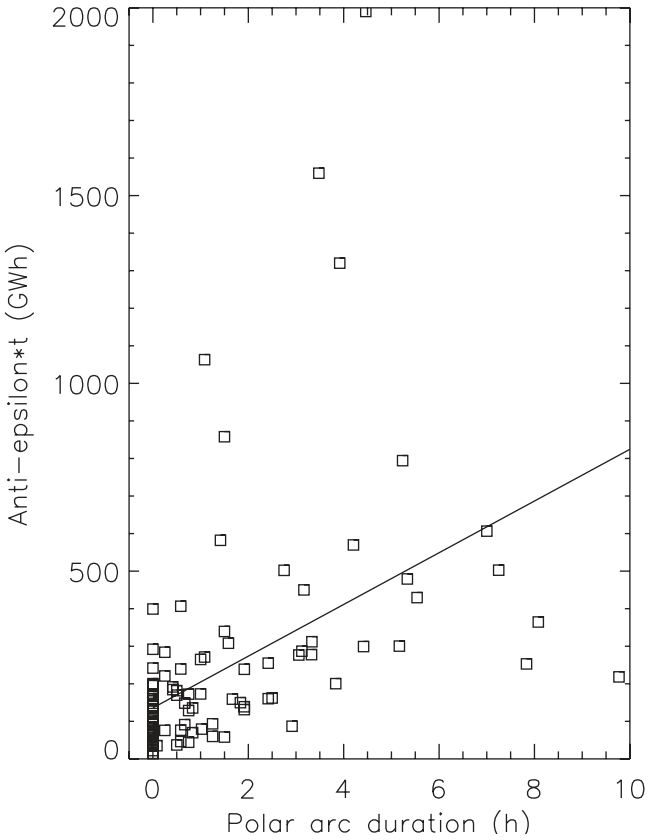

Figure 13. Each mark shows the time which is occupied by all clear arcs within one time period for which UV images are available (13 hours 45 min) versus the time integrated anti-epsilon parameter during that interval.

distribution. Looking at each clear polar arc event in detail, most cases show a temporal evolution of the anti-epsilon parameter which is similar to the change of the anti-epsilon distribution in Figure 12c. The anti-epsilon value increases to a maximum value up to hours before the event start and decreases during the event.

[55] The anti-epsilon parameter curve overlaid with all polar arc events from Figure 6 indicates already that this parameter may be used as a measure of the polar arc occurrence probability. For a better analysis it is necessary to analyze the parameter values during times where polar arcs are absent. A nearly average distribution of the solar wind parameters is found when taking the distribution of the anti-epsilon values for all time periods where no polar arc is visible on the UV imager. This is due to the fact that in most cases the anti-epsilon value is high also hours before and after the event. In Figure 13 the time integrated anti-epsilon parameter for each interval of continuous coverage by the UV imager (13 hours 45 min) is plotted versus the time during which clear polar arcs (including unclassified clear polar arc events) occur within this interval. With a correlation coefficient of 0.47 there is only a weak linear correlation between arc time and integrated anti-epsilon values. Still, Figure 13 contains other valuable information. The plot shows that of a total of 117 intervals during the entire 3 months there exist 56 intervals which do not contain any clear polar arcs at all. Nearly all of these non-arc periods (marks at $t = 0$) have integrated anti-epsilon values which do not exceed 190 GWh. Five of the seven non-arc intervals which have higher values than 190 GWh occur during the time period when the UV images have an extremely low resolution (due to the closure of the transparent MgF window at the UV imager). All intervals with integrated anti-epsilon values above 400 GWh contain at least one clear polar arc event. Excluding the seven non-arc intervals with the highest values, the maximum value for non-arc periods is 190 GWh. Around 60% of the intervals containing clear arcs have values above this limit. The distribution of different clear arc types in Figure 13 is complicated since one interval often contains several arc types, but, in general, intervals with highest anti-epsilon values contain moving or oval-aligned arcs. Multiple arcs occupy the longest interval time but have medium parameter values only. The more short-lived midnight arcs occur for even lower values and bending arcs occur during very low values, as is expected from Figure 12c.

4. Discussion

4.1. IMF B_y and B_x Dependence of Polar Arcs

[56] The study finds a clear IMF B_y control of the location and motion of clear polar arcs in the Northern Hemisphere. Nearly all clear polar arcs, separating from the side of the oval which is opposite to the direction of the IMF B_y component, move poleward in the direction of IMF B_y (bending arcs, moving arcs). The majority of the clear polar arcs occurring on the side of the oval in the direction of IMF B_y do not move considerably, they remain oval-aligned (midnight arcs, oval-aligned arcs). This confirms on a statistical basis what has been shown previously for single events: the results of *Valladares et al.* [1994] about the IMF B_y control of small-scale Sun-aligned arcs (Figure 1a) are valid also for large-scale polar arcs. As mentioned in the introduction, *Elphinstone et al.* [1990] found a slightly different IMF B_y dependence for Northern Hemisphere oval-aligned arcs (Figure 1b). While dusk arcs appear for positive IMF B_y only, dawnside arcs might appear for both signs of IMF B_y but only when IMF B_x has a sign opposite to IMF B_y. Whether or not these results are confirmed in this study is unclear, the results vary for different subsets of the clear polar arcs. Looking at oval-aligned arcs only the *Valladares et al.* [1994] results are confirmed. Including all secondary oval-aligned arcs the IMF distribution is similar to *Elphinstone et al.*'s [1990] results. Deviating from their results is the total lack of oval-aligned and secondary oval-aligned arcs for IMF B_x and B_y both being positive, although this may not be statistically significant as B_x and B_y are both positive only in 6% of the statistical time period (which is unusually rare). Our results indicate that

Figure 12. (opposite) The distribution of (a) the solar wind dynamic pressure ($\rho_i v^2$), (b) the solar wind energy flux ($(1/\mu_0)vB^2$), and (c) the anti-epsilon parameter ($vB^2 \cos^4(\theta/2)(l_0^2/\mu_0)$) as percentages of polar arc events. The figures are done in the same way as Figure 8.

only the location of the main arc is controlled by the IMF B_y sign, not the small secondary arcs which may be interpreted as part of a structured oval.

[57] The observations by *Valladares et al.* [1994] and others of small-scale Sun-aligned arcs appearing preferably on the dawn side is a feature that does not apply to larger polar arcs. In our study both small splits and clear polar arcs occur as often on the dusk as on the dawn side of the auroral oval.

[58] The more spectacular arc types, moving, midnight, and multiple arcs occur nearly exclusively for strong negative IMF B_x. This agrees with the statistical results by *Lassen and Danielsen* [1978] that small-scale Sun-aligned polar arcs occur more frequently in the Northern Hemisphere during periods of negative IMF B_x. As mentioned above, *Iijima et al.* [1984] show that the density of NBZ currents in the southern hemisphere increases linearly with positive IMF B_x. The more anti-parallel direction between the solar wind and the magnetospheric magnetic fields in the northern (southern) nightside hemisphere for negative (positive) B_x and northward B_z might have a strengthening effect on lobe reconnection in the northern (southern) hemisphere. This implies a stronger energy coupling between the solar wind and the magnetosphere on the tail lobe field lines, possibly showing up as a strengthening of the NBZ current system and in the occurrence of intense polar arcs.

4.2. A Comparison Between the Statistical Results and Different Polar Arc Models

[59] As mentioned in the introduction, the magnetotail is strongly twisted for nonzero IMF B_y if IMF B_z is positive. The degree of twisting increases downtail and toward the flanks. Since a time span of 30 to 60 min is required for the entire magnetotail to respond to an IMF direction change [*Frank and Craven*, 1988], a maximal twist should occur after an extended period of steady IMF. It is possible that the twisting increases with higher IMF magnitude (P. Janhunen, private communication, 2002). The solar wind conditions found for oval-aligned arcs support a very large and constant twisting of the entire tail. Nearly all oval-aligned arcs occur for positive IMF B_z and the IMF has been northward for at least 1 to 2 hours before the event start. The IMF is typically not varying much, often IMF B_y and B_z are equally strong, and in many cases the IMF magnitude is high. Oval-aligned arcs occur mostly on the side of the oval which maps to the plasma sheet flank reaching far into the lobes. The theory of a twisted plasma sheet with the high-latitude flank mapping to a polar arc [*Makita et al.*, 1991] fits very well to this type of clear polar arcs (Figure 2a).

[60] Moving arcs occur for similar IMF conditions as oval-aligned arcs with one major difference, they are probably triggered by an IMF B_y sign change up to an hour before the arc appears. An IMF B_y sign change from negative to positive causes in the Northern Hemisphere an arc to move from dawn to dusk and vice versa. The long time delay between the IMF B_y sign change and the arc appearance makes it probable that the development of a moving arc is connected to a large-scale tail reconfiguration caused by the IMF sign change. The statistical results support the theory proposed by *Kullen* [2000] of a rotation of the entire magnetotail which is induced by an IMF B_y sign change and makes it possible for a moving arc to appear in the ionosphere (Figure 2b). Again, northward IMF is necessary for a large tail twist to occur. The IMF B_y sign change causes the tail to change its twist first in the near-Earth tail and later in the far tail such that as an intermediate state the far tail plasma sheet maps into the high lobes of the near-Earth tail resulting in a poleward-moving arc in the ionosphere. According to this model the lifetime of a moving arc would be related to the time the magnetotail needs for a complete reconfiguration of its topology plus a possible internal magnetospheric delay. Assuming a solar wind speed of 500 km/s and a tail length of 150 R_E it takes approximately 40 min before the new IMF direction reaches the far tail. To penetrate from the flanks into the tail center takes another 45 to 60 min according to MHD simulation results [*Walker et al.*, 1999]. If we consider a further unknown time delay for field-aligned currents to reconfigure in response to the IMF change a moving arc should last for 1.5 hours or more. The lifetimes of moving arcs found in this study are extremely long, most of them last for about 2 hours, some even longer. For none of the moving arc cases was the IMF constant before and after the IMF B_y sign change. The IMF B_y component stays fairly constant but in many cases southward IMF turns occur either at the start time or during the event. An IMF B_z sign change at the arc start time probably influences the arc evolution, maybe in a similar way as for bending arcs. Interestingly, in all four cases where a secondary arc occurs during a moving arc event, a short-lived IMF B_z drop to zero takes place just before the appearance of this secondary arc. More detailed investigations are necessary to clarify the influence of an IMF B_z sign change on the motion and lifetime of moving arcs.

[61] Both the tail twist model [*Makita et al.*, 1991] and the twist rotation model [*Kullen*, 2000] propose a magnetotail topology which causes the closed field lines to map partly poleward of the main oval such that a region of closed field lines appears inside the polar cap. This field line configuration makes it possible for an auroral arc to appear poleward of the main oval boundary. The models do not explain explicitly how the field-aligned currents are generated in the tail, but both models assume that the field-aligned currents which cause the polar arc are generated in the same way as the region 1 currents of the main auroral oval, i.e., the currents are produced at the boundary between the plasma sheet and the lobes. In these models the polar arc currents have their source region in the boundary of the far tail plasma sheet near the flank which is twisted to high latitudes.

[62] Bending arcs occur for quite different solar wind conditions from the other clear polar arc types. Most bending arcs develop during IMF B_z values near zero and are connected to an IMF B_z sign change. Small splits appear during similar solar wind conditions as bending arcs. Also, nearly half of the small splits occur close to an IMF B_z sign change. Although small splits and bending arcs have an average solar wind distribution and a quite short lifetime in common, only one-third of the small splits resemble bending arcs. Even poleward moving auroral forms start to appear after an IMF B_z sign change (southward turn) [*Sandholt et al.*, 1998]. Whether or not all three arc types or subgroups of them are triggered by the same mechanism remains unclear. The theory developed by *Newell et al.* [1997] and *Chang et al.* [1998] where an IMF B_z flip causes

a jump of the dayside merging line, leading to a new region of open field lines in the high latitude ionosphere may explain the development of bending arcs. It predicts a short lifetime of the arc and its immediate appearance after an IMF B_z sign change. Some bending arcs reach far into the polar cap and last for more than 1 hour and thus they are likely to be associated with large-scale magnetotail deformations as well as the other polar arc types, which is not explicitly addressed in *Newell et al.*'s [1997] model. To extend this model to include IMF B_y sign changes as proposed by *Chang et al.* [1998] is questionable. Certainly a jump of the dayside merging line needs to be taken into account for any IMF sign change but the long time delay between the sign change and the arc occurrence and the long lifetime of the arcs indicate other mechanisms (such as magnetotail rotation).

[63] Midnight arcs develop in a completely different way from all other arc types. The arc forms from a large triangle-like bulge toward noon, within an extremely short time span, suggesting that some type of instability is involved in this process. The midnight arc model by *Rezhenov* [1995] assumes an interchange instability in the magnetotail to be responsible for the formation of an arc within the nightside oval (Figure 2c). The probability for an interchange instability increases with increasing curvature of the magnetic field lines. *Rezhenov* [1995] predicts that strong northward IMF B_z and/or strong solar wind speed during a substorm recovery is necessary for the tail magnetic field to become dipolarized and the plasma sheet to have a very short extension. These conditions agree very well with the observations of midnight arcs. All but one midnight arc occur clearly at the end of a long substorm recovery phase, during most cases the solar wind speed is very high and IMF B_z has been predominantly northward for at least 1 hour before the triangle-like bulge occurs. Midnight arcs are the only arcs occurring for clearly higher than average solar wind dynamic pressure which causes the plasma sheet to thicken such that the region of closed field lines maps to higher latitudes, resulting in a broad and contracted oval. According to *Rezhenov* [1995] the oval needs to be contracted so that the poleward oval boundary appears at very high latitudes. The UV images indicate that, just before the triangle-like bulge appears, the poleward boundary of the main oval is located on even higher latitudes than predicted by *Rezhenov* [1995]. His simulations of the motion of the poleward auroral boundary show that the oval on both sides of the arc moves considerably equatorward during the formation of the arc, which is not explicitly discussed in his paper. This phenomenon occurs in our observations as well. The whole oval widens during the formation of the midnight arc. The widening and thinning of the main oval probably reflects the recovery from a substorm to a normal state in the auroral ionosphere. The majority of the midnight arcs also involve IMF B_y and B_z sign changes. How this influences the arc formation is unclear. However, the dependence of the arc location on the sign of IMF B_y can be explained (as for oval-aligned arcs) by a twisted magnetotail.

[64] For multiple arcs the trigger mechanism is unclear. The solar wind conditions are similar to those for midnight and moving arcs. The solar wind speed and IMF magnitude are high and IMF B_z is in most cases positive. Maybe several plasma sheet filaments stretch into the tail lobes and map to different arcs, as suggested by *Huang et al.* [1987]. The changing IMF B_y and B_z components may cause the varying formations.

[65] By considering the dominant features of each clear polar arc event and examining whether common solar wind characteristics exist for arcs with a similar evolution, our statistical results indicated that primarily IMF clock angle changes are responsible for the evolution of different polar arc types. This does not exclude additional mechanisms, not revealed in this study, that may influence the polar arc evolution as well. Furthermore, it is likely that many events are the product of several mechanisms acting simultaneously on the magnetosphere-ionosphere system.

4.3. Interpretation of the Anti-Epsilon Parameter

[66] The statistical results show that a majority of the clear polar arcs occur for high solar wind speed and high IMF magnitude. One hour or more of predominantly northward IMF before event start seems to be a requirement for the arcs to occur. This holds for all clear polar arcs except for the bending arcs which more resemble the small splits. Although the overview plot in Figure 6 indicates a correlation on long timescales between high IMF values and solar wind velocities, the correlation between IMF magnitude and solar wind speed for 5 min as well as 1-hour averaged data is very low ($r \sim 0.29$) during the statistical time period. A correlation between IMF clock angle and IMF magnitude does not exist ($r = 0.09$). The correlation coefficients between IMF magnitude and solar wind velocities for polar arcs are comparable to those of the solar wind. ($r = 0.23$ for small splits and 0.41 for clear polar arcs). In a conclusion, not all arcs for which the IMF values are high occur during high solar wind velocities and vice versa.

[67] Most arcs visible in the UV images appear for a high value of the solar wind energy flux $(1/\mu_0)vB^2$. Whether a high solar wind energy flux is necessary to trigger a polar arc or whether it provides the energy for a high luminosity of polar arcs cannot be determined from this study. It is, however, likely that the magnitude of the solar wind energy flux is responsible for the rate of occurrence of intense polar arcs. A support for this assumption is that most bending arcs, which, on the average are very faint and hard to detect, do not occur for high solar wind energy flux values.

[68] In obtaining a parameter which combines the effect of high solar wind magnitude and/or solar wind speed with a northward IMF direction several combinations are possible. In this paper the anti-epsilon parameter is introduced, consisting of the well-established Akasofu-Perreault parameter with a cosine function instead of a sine function. Our statistical results show that during a time period with a high anti-epsilon parameter many and/or long-lived clear polar arcs occur. The choice for this parameter is somewhat arbitrary. The anti-epsilon parameter has only marginally higher values during polar arc events, for periods of high arc frequencies and correlation to arc lifetime (Figures 6, 12c, and 13) than other combinations of v, $|B|$ and IMF B_z northward. For example, the ϵ*-parameter by *Iijima et al.* [1984] gives fairly good correlations with arc frequencies and lifetimes as well. As mentioned above, this parameter is strongly correlated to the peak current density of NBZ currents in the

dayside polar cap. The connection between the anti-epsilon parameter and the polar arc current densities is not investigated here. But the similarity to the ϵ*-parameter suggests that the anti-epsilon parameter has a strong correlation with the current density of clear polar arcs as well.

[69] Another way to interpret the anti-epsilon parameter can be found from its connection to substorms. A negative correlation between AE index and polar arc occurrence has been shown previously [*Ismail et al.*, 1977; *Lassen and Danielsen*, 1989]. The connection between the Akasofu-Perreault epsilon parameter and the AE index is well-known. This means that for a high anti-epsilon value the AE index is low. It is commonly believed that during southward IMF solar wind energy is stored inside the magnetotail which is released periodically via substorm processes. Our suggestion is that for high anti-epsilon values (low AE but high solar wind energy flux) the energy coupling process is different, the energy is not stored inside the magnetotail but large tail deformations take place which create the closed field line topology necessary for polar arcs to occur.

5. Summary

[70] We present a statistical study of over 200 polar arcs identified utilizing the Polar UV imager. Solar wind data from the ACE satellite are examined in order to determine a possible solar wind control of these arcs. A strong IMF control of clear polar arcs is found, while small splits seem to appear nearly independent of solar wind conditions. The majority of clear polar arcs occur for northward IMF with high IMF magnitude and/or high solar wind speed.

[71] In this paper we have introduced the anti-epsilon parameter $vB^2 \cos^4(\theta/2)(l_0^2/\mu_0)$ which combines the effect of northward IMF with a high IMF magnitude and solar wind speed. A high anti-epsilon parameter means high solar wind energy flux during northward IMF conditions. Northward IMF seems to be necessary for most polar arcs to occur, with high IMF magnitude and large solar wind velocity providing the energy for a high luminosity of polar arcs. Similar to the original epsilon parameter for substorms, this parameter gives on long timescales (days) the occurrence probability for clear polar arcs. Most of the clear polar arcs occur for high values of the anti-epsilon parameter, with the highest anti-epsilon values occurring 1 to 2 hours before an event start.

[72] The clear polar arc cases are subdivided into five categories according to their spatial behavior: bending arcs, oval-aligned arcs, moving arcs, midnight arcs, and multiple arcs. The arc location for all arc types is controlled by the IMF B_y component. In the Northern Hemisphere, bending and moving arcs move toward the side of the oval pointed at by IMF B_y whereas the nonmoving arcs are located at that side of the oval from the very beginning. A clear IMF B_x dependence is found for moving, midnight, and multiple arcs. They all occur preferably during strong, negative IMF B_x. IMF clock angle changes are responsible for the formation of at least two different arc types. For each of the arc types there exist a set of favorable solar wind conditions which are listed below:

1. Bending arcs have similar characteristics to those of small splits. Bending arcs occur during average IMF conditions with IMF B_z fluctuating around zero and for slightly higher solar wind velocities than average. They are probably initiated by an IMF B_z sign change. They appear quite often but are short-lived and faint.

2. Oval-aligned arcs are a common northward IMF phenomenon occurring for high IMF magnitude, often for steady IMF with IMF B_z and B_y components having similar magnitudes. They persist from tens of minutes up to hours.

3. Moving arcs occur during IMF conditions with a strong northward component and generally large solar wind speed and IMF magnitude. They usually develop up to an hour after a large-scale IMF B_y sign change and last for several hours.

4. Midnight arcs occur for high solar wind speed and solar wind dynamic pressure with varying IMF B_y and B_z and at least 1 hour of predominantly northward IMF before a large triangle-like bulge appears out of which a midnight arc develops. All midnight arcs develop at the end of a substorm recovery phase and last up to some hours.

5. Multiple arcs occur during high solar wind speed and magnitude with positive IMF B_z and varying IMF B_y and B_z. What triggers the appearance of each arc in a multiple arc event remains unclear.

[73] The results presented in this statistical study show clearly that the occurrence and evolution of polar arcs is determined to a large extent by the solar wind energy and IMF orientation. Especially the latter seems to play a major role in reorganization of the magnetosphere which is reflected in the change of the high latitude auroral precipitation pattern.

[74] **Acknowledgments.** The work at University of Washington was supported in part by the research grant NAG 5-3170 of the National Aeronautics and Space Administration. The work at the University of Texas at Dallas was supported by NSF grant ATM9814144. We also want to thank N. Ness at Bartol Research Institute, D.J. McComas at Los Alamos National Laboratory, and the CDAWeb for providing ACE solar wind data.

References

Akasofu, S.-I., The solar wind-magnetosphere energy coupling and magnetospheric disturbances, *Planet. Space Sci.*, *28*, 495, 1980.

Bonnell, J., R. C. Elphic, S. Palfery, R. J. Strangeway, W. K. Peterson, D. Klumapar, C. W. Carlson, R. E. Ergun, and J. P. McFadden, Observations of polar cap arcs on FAST, *J. Geophys. Res.*, *104*, 12,669, 1999.

Brittnacher, M., M. Fillingim, G. Parks, G. Germany, and J. Spann, Polar cap area and boundary motion during substorms, *J. Geophys. Res.*, *104*, 12,251, 1999.

Chang, S.-W., et al., A comparison of a model for the theta aurora with observations from Polar Wind and SuperDARN, *J. Geophys. Res.*, *103*, 17,367, 1998.

Cowley, S. W. H., Magnetospheric asymmetries associated with the y-component of the IMF, *Planet. Space Sci.*, *29*, 79, 1981.

Craven, J. D., L. A. Frank, C. T. Russell, E. J. Smith, and R. P. Lepping, Global auroral responses to magnetospheric compressions by shocks in the solar wind: Two case studies, in *Solar Wind–Magnetosphere Coupling*, edited by Y. Kamide and J. A. Slavin, p. 367, Terra Sci., Tokoyo, 1986.

Craven, J. D., L. A. Frank, J. S. Murphree, L. A. Frank, and L. L. Cogger, Simultaneous optical observations of transpolar arcs in the two polar caps, *Geophys. Res. Lett.*, *18*, 2297, 1991.

Cumnock, J. A., et al., Evolution of the global aurora during positive IMF B_z and varying IMF B_y conditions, *J. Geophys. Res.*, *102*, 17,489, 1997.

Cumnock, J. A., J. R. Sharber, R. A. Heelis, L. G. Blomberg, G. A. Germany, J. F. Spann, and W. R. Coley, Interplanetary magnetic field control of theta aurora development, *J. Geophys. Res.*, doi:10.1029/2001JA009126, in press, 2002.

Elphinstone, R. D., K. Jankowska, J. S. Murphree, and L. L. Cogger, The configuration of the auroral distribution for interplanetary magnetic field B_z northward, 1, IMF B_x and B_y dependencies as observed by the Viking satellite, *J. Geophys. Res.*, *95*, 5791, 1990.

Frank, L. A., and J. D. Craven, Imaging results from Dynamics Explorer 1, *Rev. Geophys.*, *26*, 249, 1988.
Frank, L. A., J. D. Craven, J. L. Burch, and J. D. Winningham, Polar view of the Earth's aurora with dynamic explorer, *Geophys. Res. Lett.*, *9*, 1001, 1982.
Frank, L. A., J. D. Craven, and R. L. Rairden, Images of the Earth's aurora and geocorona from the Dynamics Explorer mission, *Adv. Space Res.*, *5*(4), 53, 1985.
Frank, L. A., et al., The theta aurora, *J. Geophys. Res.*, *91*, 3177, 1986.
Gusev, M. G., and O. A. Troshichev, Hook-shaped arcs in dayside polar cap and their relationship to the IMF, *Planet. Space Sci.*, *34*, 489, 1986.
Gussenhoven, M. S., Extremely high-latitude auroras, *J. Geophys. Res.*, *87*, 2401, 1982.
Gussenhoven, M. S., and E. G. Mullen, Simultaneous relativistic electron and auroral particle access to the polar caps during interplanetary magnetic field B_z northward: A scenario for an open field line source of auroral particles, *J. Geophys. Res.*, *94*, 17,121, 1989.
Hones, E. W., Jr., J. D. Craven, L. A. Frank, D. S. Evans, and P. T. Newell, The horse-collar aurora: A frequent pattern of the aurora in quiet times, *Geophys. Res. Lett.*, *16*, 37, 1989.
Huang, C. Y., L. A. Frank, W. K. Peterson, D. J. Williams, W. Lennartson, D. G. Michell, R. C. Elphic, and C. T. Russell, Filamentary structures in the magnetotail lobes, *J. Geophys. Res.*, *92*, 2349, 1987.
Huang, C. Y., J. D. Craven, and L. A. Frank, Simultaneous observations of a theta aurora and associated magnetotail plasmas, *J. Geophys. Res.*, *94*, 10,137, 1989.
Iijima, T., and T. A. Potemra, The relationship between interplanetary quantities and Birkeland current densities, *Geophys. Res. Lett.*, *4*, 442, 1982.
Iijima, T., T. A. Potemra, L. J. Zanetti, and P. F. Bythrow, Large-scale Birkeland currents in the dayside polar region during strongly northward IMF: A new Birkeland current system, *J. Geophys. Res.*, *89*, 7441, 1984.
Ismail, S., and C.-I. Meng, A classification of polar cap auroral arcs, *Planet. Space Sci.*, *30*, 319, 1982.
Ismail, S., D. D. Wallis, and L. L. Cogger, Characteristics of polar cap sun-aligned arcs, *J. Geophys. Res.*, *82*, 4741, 1977.
Kaymaz, Z., G. L. Siscoe, J. G. Luhmann, R. P. Lepping, and C. T. Russell, Interplanetary magnetic field control of magnetotail magnetic field geometry: IMP 8 observations, *J. Geophys. Res.*, *99*, 11,113, 1994.
Kullen, A., The connection between transpolar arcs and magnetotail rotation, *Geophys. Res. Lett.*, *27*, 73, 2000.
Kullen, A., and L. G. Blomberg, The influence of IMF B_y on the mapping between the Earth's magnetotail and its ionosphere, *Geophys. Res. Lett.*, *23*, 256, 1996.
Lassen, K., and C. Danielsen, Quiet time pattern of auroral arcs for different directions of the interplanetary magnetic field in the yz-plane, *J. Geophys. Res.*, *83*, 5277, 1978.
Lassen, K., and C. Danielsen, Distribution of auroral arcs during quiet geomagnetic conditions, *J. Geophys. Res.*, *94*, 2587, 1989.
Makita, K., C. I. Meng, and S. I. Akasofu, Transpolar auroras, their particle precipitation, and IMF B_y component, *J. Geophys. Res.*, *96*, 14,085, 1991.
McEwen, D. J., and Y. Zhang, A continuous view of the dawn-dusk polar cap, *Geophys. Res. Lett.*, *27*, 477, 2000.
Meng, C.-I., Polar cap arcs and the plasma sheet, *Geophys. Res. Lett.*, *8*, 273, 1981.
Milan, S. E., M. Lester, S. W. H. Cowley, and M. Brittnatcher, Convection and auroral signatures of transient magnetic flux transfer at the magnetopause, *J. Geophys. Res.*, *105*, 15,741, 2000.
Murphree, J. S., and L. L. Cogger, Observed connections between apparent polar cap features and the instantaneous diffuse auroral oval, *Planet. Space Sci.*, *29*, 1143, 1981.
Murphree, J. S., C. D. Anger, and L. L. Cogger, The instantaneous relationship between polar cap and oval auroras at times of northward interplanetary magnetic field, *Can. J. Phys.*, *60*, 349, 1982.
Newell, P. T., D. Xu, C.-I. Meng, and M. G. Kivelson, Dynamical polar cap: A unifying approach, *J. Geophys. Res.*, *102*, 127, 1997.
Owen, C. J., J. A. Slavin, I. G. Richardson, N. Murphy, and R. J. Hynds, Average motion, structure and orientation of the distant magnetotail determined from remote sensing of the edge of the plasma sheet boundary layer with $E > 35$ keV ions, *J. Geophys. Res.*, *100*, 185, 1995.
Perreault, P., and S. I. Akasofu, Study of geomagnetic storms, *Geophys. J. R. Astron. Soc.*, *54*, 547, 1978.
Peterson, W. K., and E. G. Shelley, Origin of the plasma in a cross-polar cap auroral feature (theta aurora), *J. Geophys. Res.*, *89*, 6729, 1984.
Rairden, R. L., and S. B. Mende, Properties of 6300-A auroral emission at south pole, *J. Geophys. Res.*, *94*, 1402, 1989.
Richmond, A. D., Ionospheric electrodynamics using magnetic apex coordinates, *J. Geophys. Res.*, *47*, 191, 1995.
Rezhenov, B. V., A possible mechanism for theta aurora formation, *Ann. Geophys.*, *13*, 698, 1995.
Sandholt, P. E., C. J. Farrugia, J. Moen, O. Noraberg, B. Lybekk, T. Sten, and T. Hansen, A classification of dayside auroral forms and activities as a function of interplanetary magnetic field orientation, *J. Geophys. Res.*, *103*, 23,325, 1998.
Slinker, S. P., J. A. Fedder, D. J. McEwen, Y. Zhang, and J. G. Lyon, Polar cap study during northward interplanetary magnetic field on 19 January 1998, *Phys. Plasmas*, *8*, 1119, 2001.
Torr, M. R., et al., A far ultraviolet imager for the international solar-terrestrial physics mission, *Space Sci. Rev.*, *71*, 329, 1995.
Tsyganenko, N. A., A magnetospheric magnetic field model with a warped tail current sheet, *Planet. Space Sci.*, *37*, 5, 1989.
Valladares, C. E., H. C. Carlson, Jr., and K. Fukui, Interplanetary magnetic field dependency of stable sun-aligned polar cap arcs, *J. Geophys. Res.*, *99*, 6247, 1994.
Walker, R. J., R. L. Richard, T. Ogino, and M. Ashour-Abdalla, The response of the magnetotail to changes in the IMF orientation: The magnetotail's long memory, *Phys. Chem. Earth, Part C*, *24*, 221, 1999.
Zhu, L., R. W. Schunk, and J. J. Sojka, Polar cap arcs: A review, *J. Atmos. Sol.-Terr. Phys.*, *59*, 1087, 1997.

L. G. Blomberg and A. Kullen, Royal Institute of Technology, Alfvén Laboratory, 10044 Stockholm, Sweden. (Lars.Blomberg@alfvenlab.kth.se; kullen@plasma.kth.se)

M. Brittnacher, Department of Earth and Space Sciences, University of Washington, Box 351650, Seattle, WA 98195, USA. (britt@geophys.washington.edu)

J. A. Cumnock, Center for Space Sciences, University of Texas at Dallas, Richardson, TX 75080, USA. (cumnock@utdallas.edu)